# CENTER FOR INFRASTRUCTURE ENGINEERING STUDIES

**Assessment of Bridge Technologies through Field Testing: In-situ load testing of Bridges B-20-133 and B-20-134, Fond du Lac, WI**


**By**

**Eli Hernandez**
**Nestore Galati**
**Antonio Nanni**

**UTC R133A**

**Technical Report Documentation Page**

| 1. Report No.<br><br>UTC R133A | 2. Government Accession No. | 3. Recipient's Catalog No. |
|---|---|---|
| 4. Title and Subtitle<br><br>In-Situ Load Testing Of Bridges B-20-133 And B20-134<br>Fond Du Lac, Wi | | 5. Report Date<br><br>December 2005 |
| | | 6. Performing Organization Code |
| 7. Author/s<br><br>Eli Hernandez, Nestore Galati, and Antonio Nanni | | 8. Performing Organization Report No.<br><br>00001342 |
| 9. Performing Organization Name and Address<br><br>Center for Infrastructure Engineering Studies/UTC program<br>University of Missouri - Rolla<br>223 Engineering Research Lab<br>Rolla, MO 65409 | | 10. Work Unit No. (TRAIS) |
| | | 11. Contract or Grant No.<br><br>DTRS98-G-0021 |
| 12. Sponsoring Organization Name and Address<br><br>U.S. Department of Transportation<br>Research and Special Programs Administration<br>400 7th Street, SW<br>Washington, DC 20590-0001 | | 13. Type of Report and Period Covered<br><br>Final |
| | | 14. Sponsoring Agency Code |

15. Supplementary Notes

16. Abstract

The scope of this project is the evaluation of two twin bridges having numbers B-20-133 and B-20-134, respectively, located on US Highway 151 over State Highway 26, near the City of Waupun in Fond du Lac County, Wisconsin. Bridge B-20-133 was constructed utilizing a cast in place Fiber Reinforced Polymer (FRP) Reinforced Concrete (RC) Deck while Bridge B-20-134 was built using a conventional cast in place RC deck.

To better evaluate the load-carrying capacity of the bridges, a nondestructive field test was conducted. The bridges were tested statically using six dump trucks. The bridges deflections were measured using a Robotic Tacheometry System (RTS), while the strains at critical locations were measured by means of electrical resistive strain gages. The RTS is a noncontact deflection measurement technique that offers the capability to measure the spatial coordinates of discrete points on a structure in three dimensions without having to touch the object.

A Finite Element Method (FEM) Model was developed to represent the behavior of the bridge and was used to determine the actual load rating of the structure and its safety over time. The comparison between analytical results obtained according to AASTHO standard specifications, FEM modeling and experimental allowed establishing a good understanding of the bridges performance.

| 17. Key Words<br><br>assessment, bridge monitoring, concrete deck, frp, high performance steel, in-situ load test, static load test, structural evaluation, total station. | 18. Distribution Statement<br><br>No restrictions. This document is available to the public through the National Technical Information Service, Springfield, Virginia 22161. | | |
|---|---|---|---|
| 19. Security Classification (of this report)<br><br>unclassified | 20. Security Classification (of this page)<br><br>unclassified | 21. No. Of Pages | 22. Price |

Form DOT F 1700.7 (8-72)

**ACKNOWLEDGMENTS**

# TABLE OF CONTENTS

# LIST OF FIGURES

## LIST OF TABLES

# NOTATIONS

$A$      :   Cross sectional area of girder, $mm^2$

$A_b$      :   Cross sectional area of concrete barrier, $mm^2$

$E_c$      :   Modulus of elasticity of concrete girder, MPa

$E_{cs}$      :   Modulus of elasticity of girder, MPa

$I$      :   Moment of inertia of the concrete girder section, $mm^4$

$K_g$      :   Longitudinal stiffness parameter, $mm^4$

$L$      :   Span length, mm

$P_1$      :   Dump truck front axle load, kN

$P_2$      :   Dump truck rear axle load, kN

$S$      :   Girder spacing, mm

$e_g$      :   Distance between center of gravity of girder section and concrete deck, mm

$f_y$      :   Steel yield strength, MPa

$m$      :   Multiple presence factor

$t_s$      :   Thickness of concrete deck, mm

$w_{overhang}$   :   Overhang width from exterior girder center line, mm

$\delta_i$      :   Deflection of $i$th girder, mm

$GDF$      :   Girder distribution factor

$\theta$      :   Skew angle

$d_e$      :   Distance between center of exterior girder and interior edge of barrier

$n$      :   Modular ratio between beam and slab, $n = \dfrac{E_s}{E_{cs}}$

# 1 INTRODUCTION

## 1.1 Background

### 1.1.1 Pultruded Grid and Stay-in-Place (SIP) Form Panels for the Rapid Construction of Bridge Decks

The Federal Highway Administration (FHWA) has reported that in the United States there are over half a million of bridges in service and that more than twenty five percent of these bridges are considered deficient. Among the principal reasons ascribed to the structural deterioration of these existing bridges are corrosion of reinforcing steel due to chloride ion penetration, aging of materials and inadequate maintenance of the infrastructure. Deficient bridges are usually posted, repaired or replaced causing elevated costs to the nation. The impact of the economic and social costs associated with bridge deck rehabilitation and replacement presents a necessity to develop durable structural systems that can be rapidly installed.

To date, extensive research has demonstrated the effectiveness of using pultruded FRP gratings as internal reinforcement of bridge decks (Bank et al. 1992, Bank and Xi 1993, 1995). Together with durability, the key feature of the proposed solutions is the quickness of installation. This is ensured by no need of tied-in-place reinforcement, lightweight of the prefabricated gridform panels (about 23 kg/m2, 4.7 lb/ft2), and the use of Stay-In-Place (SIP) formwork (Bank et al. 2004). Similarly, the use of pultruded Glass FRP (GFRP) bars as internal reinforcement of concrete decks and railings ideally eliminates the problem of corrosion and also simplifies the installation process (Bradberry 2001, Buth et al. 2003, El-Salakawi et al. 2003).

Extensive research and development work funded through the FHWA Innovative Bridge Research and Construction (IBRC) project demonstrated the feasibility of using FRP pultruded gratings and SIP form panels for the rapid construction of steel-free bridge decks. This technology was recently implemented in pilot field applications in Wisconsin, U.S.A. (Berg, 2004). The proposed system consists in using FRP rebars in conjunction with FRP grids and FRP SIP form panels that offset the cost of the FRP material by eliminating the formwork spanning between girders.

### 1.1.2 Diagnostic Load Testing

Field-testing is an important topic in the validation of innovative infrastructure as well as in the assessment of deficient structures. There is a need for accurate and inexpensive diagnostics methods that allow the determination of the actual load carrying capacity of the structures. In order to predict the response of a bridge, its evaluation must accurately expose its present load carrying capacity and should predict loads and any further changes of its capacity (deterioration) during the applicable time life span.

Experimental load testing on a bridge can be categorized as either as diagnostic or proof test. In a diagnostic test, a predetermined load, typically near the bridge's rated capacity, is placed at several different locations along the bridge and its behavior is obtained. The measured response is used to develop a numerical model of the bridge to estimate its maximum allowable load. In a proof test, incremental loads are applied to the bridge until either a target load is reached or a predetermined limit state is exceeded. Using the maximum load reached, the capacity of the

bridge can be determined. While diagnostic tests provide only an estimate of a bridge's capacity, they have several practical advantages including a lower cost, a shorter testing time, and less disruption to traffic. Because of these advantages, diagnostic testing was used in this evaluation. Frequently, diagnostic load tests reveal strength and serviceability characteristics that exceed predicted parameters. Usually, these parameters are very conservative in predicting lateral load distribution factors and the influence of other structural attributes. As a result, the predicted rating factors are typically conservative (Chajes et al. 1997). This difference can be attributed to the existence of "beneficial factors", such as parapet stiffening, contribution of secondary members, diaphragm action, concrete hardening, unintended composite action and unintended bearing restraints that are usually neglected in a new bridge design and analytical capacity rating (Cai et al. 2003).

A difficulty in the testing and evaluation of bridges in the field is the measurement of vertical deflection. The use of instruments such as mechanical dial gages, linear potentiometers, linear variable differential transducers (LVDTs), and other similar types of deflection transducers is usually not feasible. Access under a bridge structure sometimes is limited due to several conditions; for instance, the necessity to erect temporary supports to mount and setup the measurement instruments to the ground or the presence of a natural creek under the bridge. These difficulties can be eliminated by using a Robotic Tacheometry System (RTS), which is a noncontact deflection measurement technique. RTS offers the capability to measure the spatial coordinates of discrete points on a bridge in three dimensions without having to touch the structure. In this research, the RTS was used to monitor the deflection of points located along the bridge girder.


### 1.1.3   Robotic Tacheometry Systems in Diagnostic Load Tests

RTS also called Total stations have been used to measure the movement of structures and natural processes with good results (Hill and Sippel 2002; Kuhlmann and Glaser 2002).  Leica Geosystems quotes accuracies of better than 1mm for their bridge and tunnel surveys where a remote system is used to log measurements six times daily via a modem, with measurements still possible at peak times.  Kuhlmann and Glaser (2002) used a reflectorless total station to monitor the long-term deformation of bridges.  Measurements were taken of the whole bridge every six years and statistical tests were used to confirm if the points had moved.  Hill and Sippel (2002) used a total station and other sensors to measure the deformation of the land in a landslide region. Merkle (2004) used the total station as part of a 5-year monitoring program for the in-situ load testing prior to and after the strengthening of five existing concrete bridges, geographically spread over three Missouri Department of Transportation (MODOT) districts. There are advantages and disadvantages of using a total station for dynamic deformation monitoring.  The advantages include the high accuracy as quoted above, the automatic target recognition which provides precise target pointing (Hill and Sippel 2002) and the possibility of measuring indoors and in urban canyons (Radovanovic and Teskey 2001).  The disadvantages include the low sampling rate (Meng 2002), problems with measurement in adverse weather conditions (Hill and Sippel 2002) and the fact that a clear line of sight is needed between the total station and the prism.

Radovanovic and Teskey (2001) conducted experiments to compare the performance of a robotic total station with GPS.  This experiment was conducted because GPS is not an option in many

application areas such as indoors.  Total stations are now capable of automatic target recognition and they can track a prism taking automatic measurements of angles and distances once lock has been established manually.  It was found that the total station performed better than GPS in a stop and go situation, where measurements were taken of a moving object only when it was stationary.  In a completely kinematic situation, GPS performed the best.  It was found that there were two main problems with the total station in kinematic mode. These problems were basically a low EDM accuracy caused by a ranging error that was linearly dependent upon the line of sight velocity, and an uneven sampling rate over time worsened by no time tagging.

## 1.2    Bridges Description

The bridges under investigation are located north of Waupun, Wisconsin on U.S. Highway 151 as an overpass over State Highway 26 Service Road. Both bridges were completed during July 2003 and were designed for the controlling truck load known as MS18 with military 106 KN tandem axles. Each bridge is 12.75 m wide and carries two lanes of traffic. The superstructure of each bridge consists of two continuous spans having a length of 32.81 m,  a skew angle of $32^o$ 10' and a central support consisting of an RC bent supported by three RC circular piers. The cross section consists of five Prestressed Concrete (PC) girders equally spaced, supporting an FRP reinforced cast in place concrete deck (Figure 1) in the case of bridge B-20-133 and a cast-in-place conventional RC deck for bridge B-20-134 (Figure 2). Cross section details of the PC girders of the bridges B-20-133 and B-20-134 are presented in Figure 1 and Figure 2 respectively (Berg 2004 gives additional details about the design and construction of the two bridges).
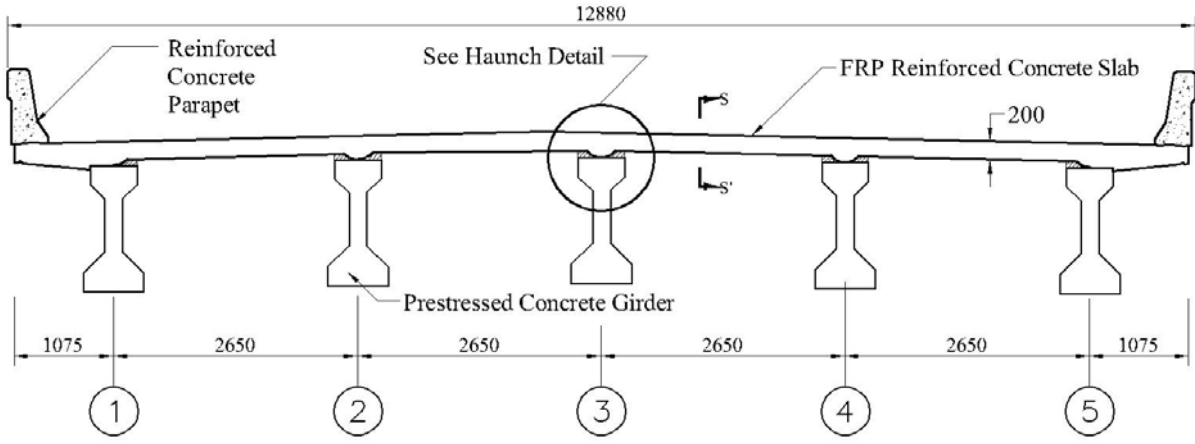
a) Cross Section of Bridge (drawing not in scale)
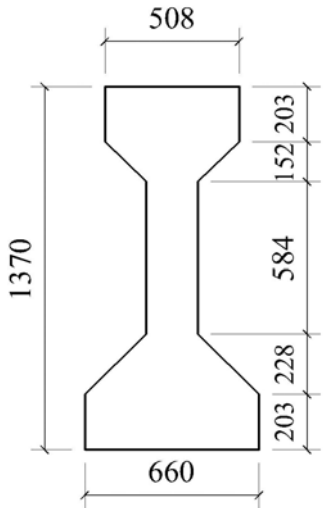


b) Cross Section of the Girders
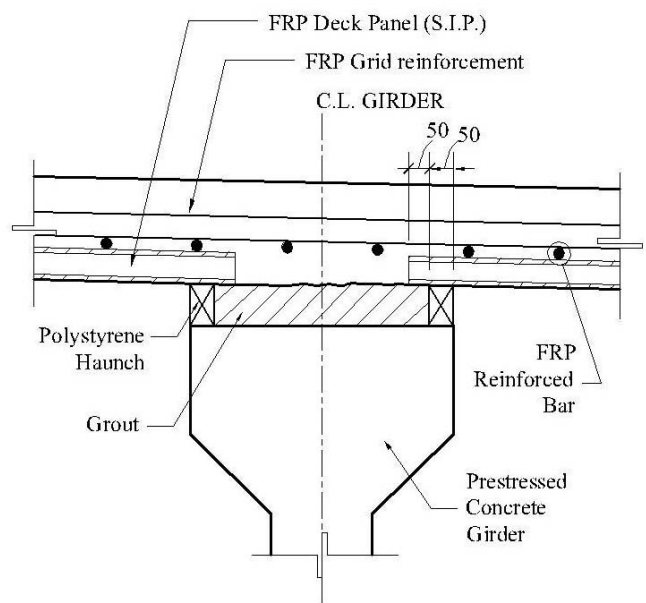


c) Haunch Detail
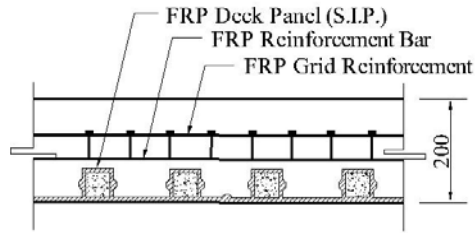


d) Detail of Section S-S' (drawing not in scale)

Figure 1 Bridge B-20-133 Details (all dimensions in mm)
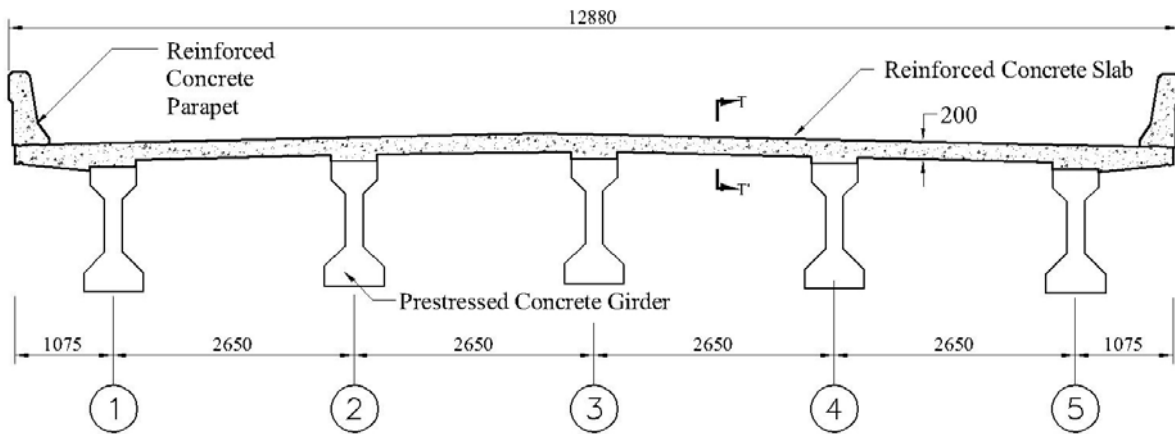
a) Cross Section of Bridge B-20-134 (drawing not in scale)
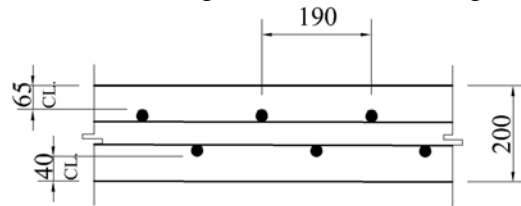


c) Detail of Section T-T' detail (drawing not in scale)

Figure 2 Bridge B-20-134 details (all dimensions in mm)

A photograph of the structure of both bridges is exhibited in Figure 3.



Figure 3 Side View Bridge B-20-133 (Front) and B-20-134 (Back)

The plan view and typical diaphragm of both bridges are detailed in Figure 4.

6
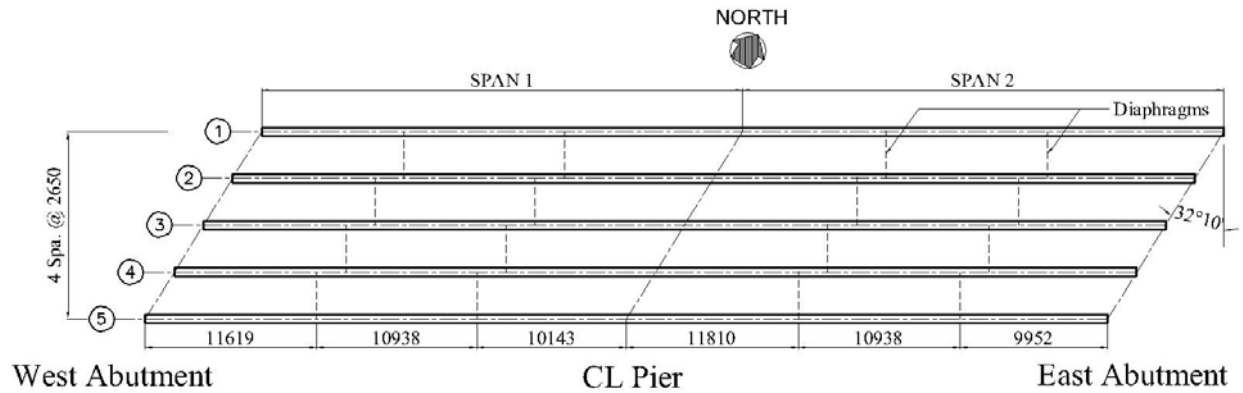
a) Plan View of Bridges B-20-133 and B-20-134
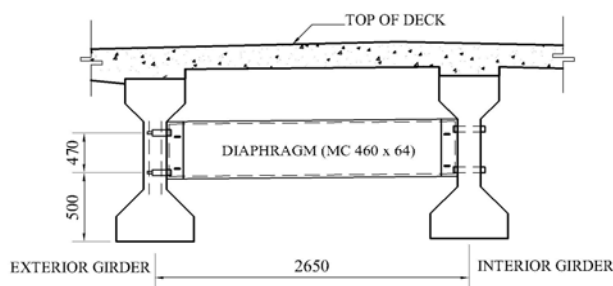


b) Typical Diaphragm (Drawing not in scale)

Figure 4  Framing Plan (all dimensions in mm)

## 1.3    Objectives

The scope of this project is the evaluation of two twin bridges built in Waupun, Wisconsin, having number B-20-133 and B-20-134. To better evaluate the load-carrying capacity of the bridges, a nondestructive field test was conducted. A comparison between analytical results obtained according to AASTHO standard specifications, FEM modeling and experimental results was carried out in order to establish a good understanding of the bridges performance.

## 1.4    Equipment Description

### 1.4.1    Total station

The RTS used in this project is a Leica TCA2003 (www.leica-geosystems.com) as shown in Figure 5. The instrument sends a laser ray to reflecting prisms (see Figure 8) mounted on the structure to be monitored. By means of a triangulation with fixed reference points placed outside the structure. The RTS can determine how much the structure has moved in a three-dimensional array with an accuracy of 0.5 sec on angular measurements and 1mm+1ppm on distance measurements, in average atmospheric conditions.

Figure 5 Total Station

For this experimental program, strain gages were also used to characterize the bridges' response. In order to read the data from the strain gages, a custom-made data acquisition system was used. The system is able to read data up to 100 Hz.

### 1.4.2   Data Acquisition System: (DAS)

The DAS is a portable unit, suitable for use in field testing of structures.  It is capable of recording 32 high-level channels of data, 16 strain channels, and 32 thermocouple channels, as well as interfacing a Leica Total Station surveying instrument (See Figure 6).



Figure 6 Data Acquisition System ("Orange Box")

The high-level channels may consist of DC LVDT's, string transducers, linear potentiometers, or any other +/- 10 Volt DC signal.  The strain channels can be used to monitor and record strain gage signals, load cells, strain-based displacement transducers, or any strain based signal.  The 32 thermocouple channels are configured for type T thermocouples.

The unit consists of a shock-mounted transport box, with removable front and rear covers. Removal of the front cover exposes the computer keyboard and LED display, as well as the front panel of the data acquisition equipment.  Removal of the back panel exposes the connector bay, where cables from all the transducers terminate.

The data acquisition system is comprised of National Instruments equipment, listed below:
1. A PXI-1010 SCXI combination unit, which houses the industrial-grade 2.2 GHz Pentium 4 computer, floppy drive, and CDR/W module;
2. A PXI-6030E Analog to Digital converter module for doing the A/D conversion in the system;
3. A pair of SCXI-1520 modules to interface strain based sensors;
4. A SCXI-1102B module for multiplexing high-level sensors;
5. A SCXI-1102B module for multiplexing thermocouple sensors;
6. I/O devices in order to connect additional peripherals and other data acquisition systems such as a Leica Total Station surveying instrument.

The entire DAS is controlled by LabVIEW software, which allows control of data rate, sensor selection and calibration, and display of the data.

## 2    FIELD EVALUATION

### 2.1    Bridge Instrumentation

### 2.1.1    Bridge B-20-133

Nineteen prisms (also called targets) were mounted along the girders in Bridge B-20-133 as shown in Figure 7.  Targets 1 to 5 and targets 7 to 11, along external Girder 1, provided the longitudinal deformed shape, while the remaining targets were distributed transversally in order to determine the distribution of loads among the girders. Two of the transversal targets, namely target 17 and 18 in Figure 7, were mounted at mid-span of the deck between Girders 1 and 2 in order to determine the deflection of the deck at these locations. Finally, three targets were mounted on tripods as reference points for triangulation and another target (target 6) was mounted on the central pier as an additional reference point.
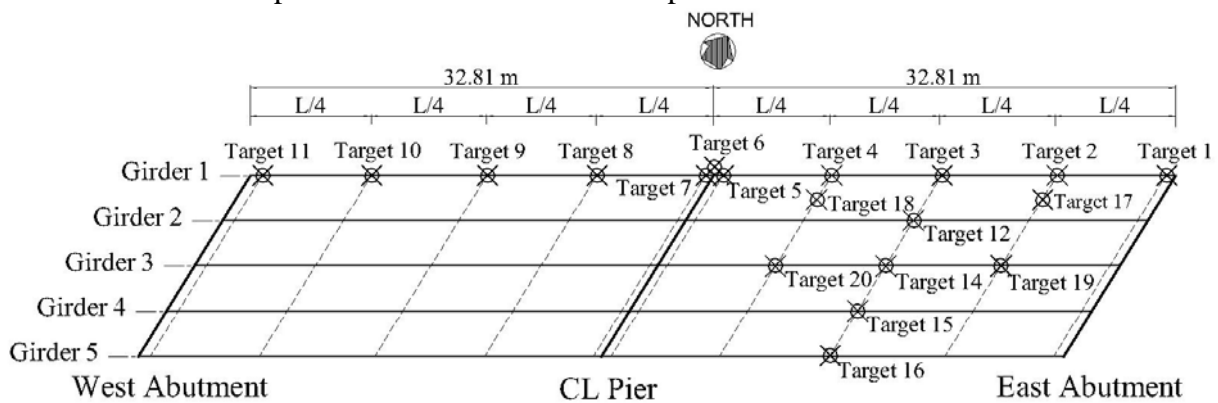


Figure 7 Target Positions: Plan View of Bridge B-20-133 (Drawing not to scale)

The targets were magnetically mounted on the structure prior to testing and this required the installation of steel plates on the structure at the corresponding positions. The steel plates were glued to the girders using an epoxy resin and, as an additional safety measure; they were also mechanically fastened by using two bolts. In the case of the prisms to be mounted underneath the deck (targets 17 and 18), a steel pipe was attached to the deck soffitt using the same procedure as for the steel plates, as shown in Figure 8.



Figure 8 Targets Mounted on Bridge Girders and Deck

The connections of steel plates and pipes to the superstructure were designed to carry their own weight plus the weight of the targets with a safety factor equal to four. However, it is advised to

remove the steel pipes from the structure no later than **December 2006** as a safety measure due to the presence of vehicular traffic underneath the bridge.

Strain gages were installed by the research team of the UW during the construction phase of the bridge, and their locations are presented in Figure 9 and Table 1 (Berg, 2004).
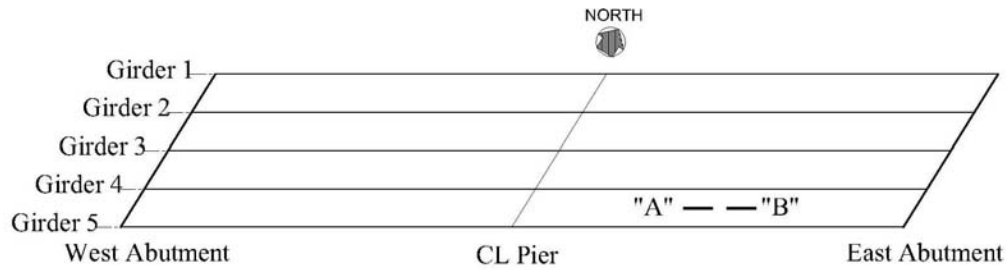
a) Strain Gage Instrumentation for 12.7 mm Diameter FRP Grid Cross Rods
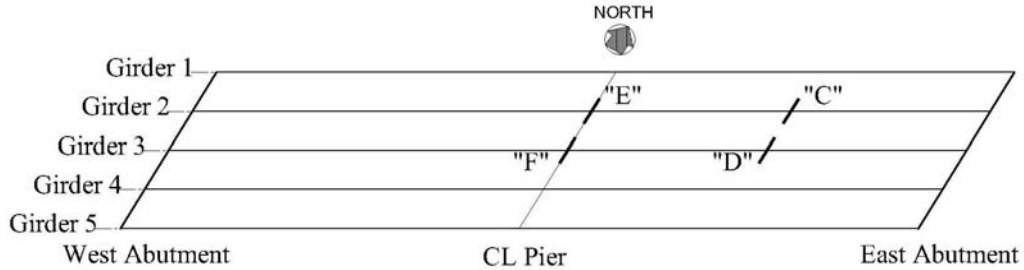
b) Strain Gage Instrumentation for 50.8 mm FRP Grid T-bars
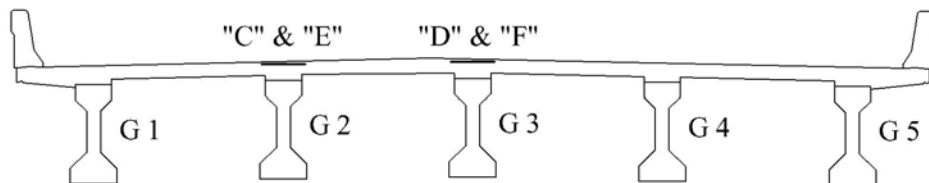
c) Cross Section of Strain Gage Instrumentation for 50.8 mm FRP Grid T-bars
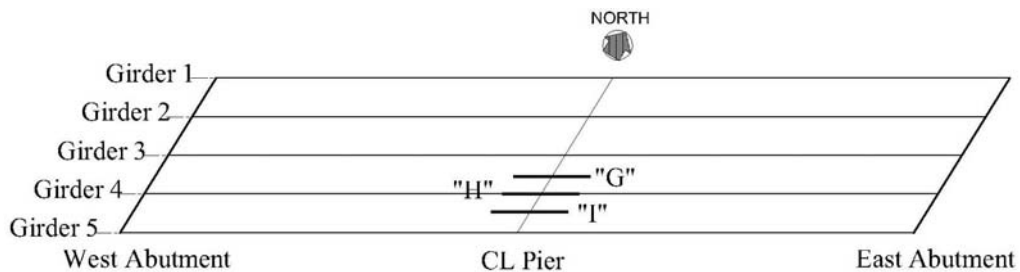
d) Strain Gage Instrumentation for 25.4 mm Diameter FRP Rebars

Figure 9 Strain Gages Location for Bridge B-20-133 (Berg, 2004)

Table 1 Strain Gage Locations for Bridge B-20-133 (Berg, 2004)

| Gage | Channel | Material | Location |
|------|---------|----------|----------|
| A | 5 | FRP Grid 12.7 mm Diameter Cross Rod | Near mid-span of Span 2. Near mid-span of deck panel. Directly above middle valley between tubular corrugations of deck panel. Between Girders 4 and 5. |
| B | 6 | FRP Grid 12.7 mm Diameter Cross Rod | Near mid-span of Span 2. Near mid-span of deck panel. Directly above lap splice between deck panels. Between Girders 4 and 5. |
| C | 2 | FRP Grid 50.8 mm T-bar | Near mid-span of Span 2 at the centerline of Girder 2 |
| D | * | FRP Grid 50.8 mm T-bar | Near mid-span of Span 2 at the centerline of Girder 3 |
| E | 7 | FRP Grid 50.8 mm T-bar | Over the center pier at the centerline of Girder 2 |
| F | 8 | FRP Grid 50.8 mm T-bar | Over the center pier at the centerline of Girder 3 |
| G | 4 | 25.4 mm FRP Rebar | Over the center pier between Girders 3 & 4 |
| H | * | 25.4 mm FRP Rebar | Over the center pier at the centerline of Girder 4 |
| I | 3 | 25.4 mm FRP Rebar | Over the center pier between Girders 4 & 5 |
| * Gage did not work during load test | | | |

The load test was carried out by using six fully loaded H-20 dump trucks that were weighted before test. The sketch in Figure 10b shows the average dimensions of the trucks used for the load test. All trucks were weighted before testing and coded with a number. Table 2 summarizes the weights and load distribution between front and rear axles of the trucks used for the test. The value $P_2$ in Table 2 corresponds to the weight of each of the rear axle, which means that the total rear weight of the truck will be twice $P_2$. The bridge was loaded using a train of trucks and the average distance between the front axle of a truck and the rear axle of the truck in front of it was 2.5 m.
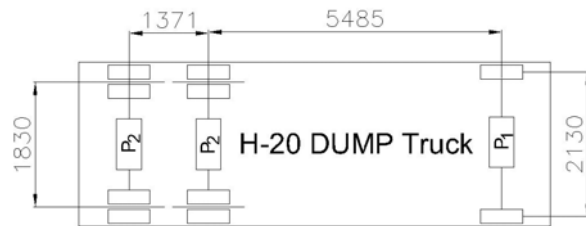


a) Trucks on Site                b) Trucks Geometry (all dimensions in mm)

Figure 10 H-20 Dump Trucks

Table 2 Weight of Trucks Used for Test of Bridge B-20-133

| Truck Code | Total Weight (kN) | Front Axle ($P_1$) (kN) | Each Rear Axle ($P_2$) (kN) |
|---|---|---|---|
| 1 | 325.6 | 80.78 | 122.4 |
| 2 | 324.3 | 113.0 | 105.7 |
| 3 | 332.7 | 113.9 | 109.4 |
| 4 | 331.4 | 108.1 | 111.7 |
| 5 | 337.2 | 107.7 | 114.8 |
| 6 | 343.2 | 115.2 | 114.0 |

## 2.1.2 Bridge B-20-134

Nineteen prisms (also called targets) were mounted along the girders of Bridge B-20-134 as shown in Figure 11. For this bridge, the targets were installed on Girder 5 because of the RTS' visibility difficulty to read data if the targets would have been located on Girder 1. For this bridge, targets 1 to 5 and targets 6 to 10, along external Girder 5, provided its longitudinal deformed shape, while the remaining targets were distributed transversally to determine the distribution of the loads among the girders. Three of the transversal targets, namely target 15 through 17 in Figure 11, were mounted underneath the deck between Girders 4 and 5 to determine the deflection of the deck. As for the case of Bridge B-20-133, three reference points were also used for triangulation.
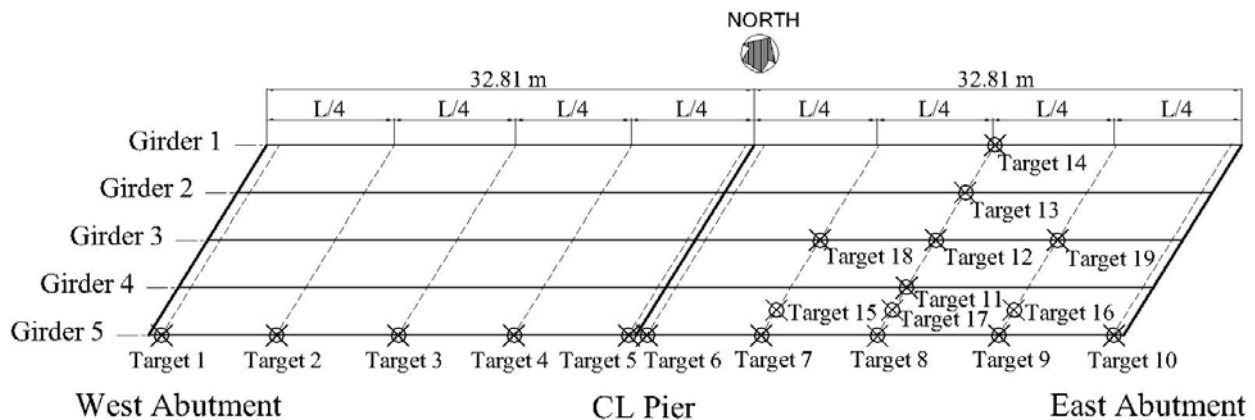


Figure 11 Target Positions of Bridge B-20-134: Plan View (Drawing not in scale)

Strain gages were installed during the construction phase of the bridge and their location are displayed in the sketch of Figure 12 and a summary of the steel reinforcement the strain gages were installed is presented in Table 3 (Berg, 2004).
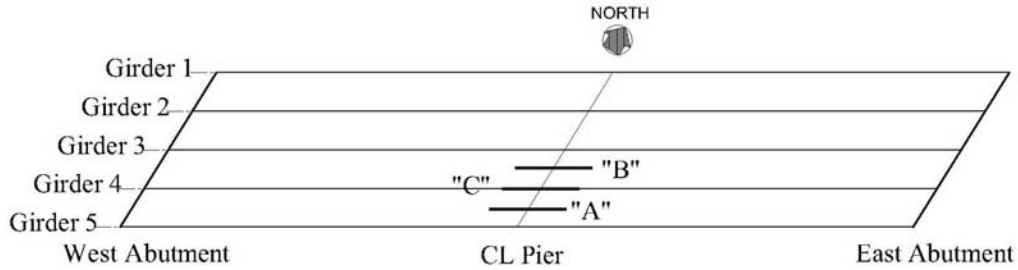
a) Instrumentation Plan for Longitudinal Reinforcement
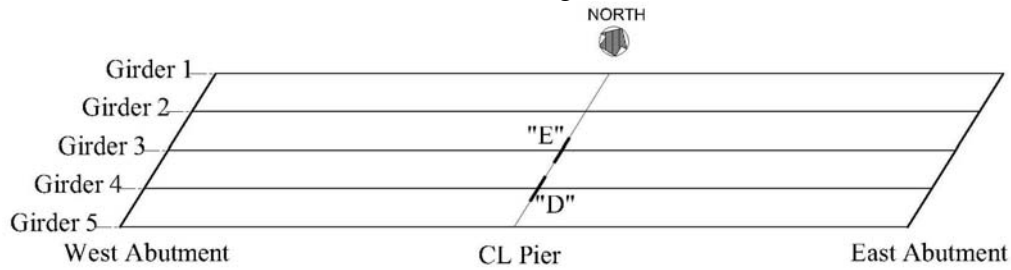


b) Instrumentation Plan for Transverse Reinforcement

Figure 12 Strain Gages Location for Bridge B-20-134 (Berg, 2004)

Table 3 Strain Gage Locations for Bridge B-20-134 (Berg, 2004)

| Gage | Material | Location |
|------|----------|----------|
| A | 9.5 mm Steel Rebar | Over the center pier between Girder 4 & 5 |
| B | 9.5 mm Steel Rebar | Over the center pier between Girder 3 & 4 |
| C | 9.5 mm Steel Rebar | Over the center pier at the center line of Girder 4 |
| D | 9.5 mm Steel Rebar | Over the center pier at Girder 4 |
| E | 9.5 mm Steel Rebar | Over the center pier at Girder 3 |

For this bridge, the load test was carried out by using six fully loaded H-20 dump trucks as shown in Figure 10. All trucks were weighted before load testing and coded with a number. Table 4 summarizes the weights and load distribution between front and rear axles of the trucks used for the test. The train of trucks and the average distance between the front axle of a truck and the rear axle of the truck in front of it was 2.59 m (8.5 ft).

Table 4 Trucks Used for Test of Bridge B-20-134

| Truck Code | Total Weight (kN) | Front Axle ($P_1$) (kN) | Each Rear Axle ($P_2$) (kN) |
|------------|-------------------|-------------------------|------------------------------|
| 1 | 337.8 | 110.0 | 113.9 |
| 2 | 309.4 | 98.0 | 105.7 |
| 3 | 345.7 | 117.9 | 113.9 |
| 4 | 329.9 | 93.5 | 118.2 |
| 5 | 319.2 | 115.8 | 101.7 |
| 6 | 323.8 | 96.2 | 113.8 |

14

## 2.2   Load Testing Methodology

### 2.2.1   Bridge B-20-133

Three load configurations identified as Test 1, 2 and 3 were planned to produce maximum deflections.  For Test 1, two trains of trucks (three trucks each train) were transversally placed and centered on Girders 2 and 4 (see Figure 13). This configuration was intended to produce the maximum deflection of the girders at Span 2.
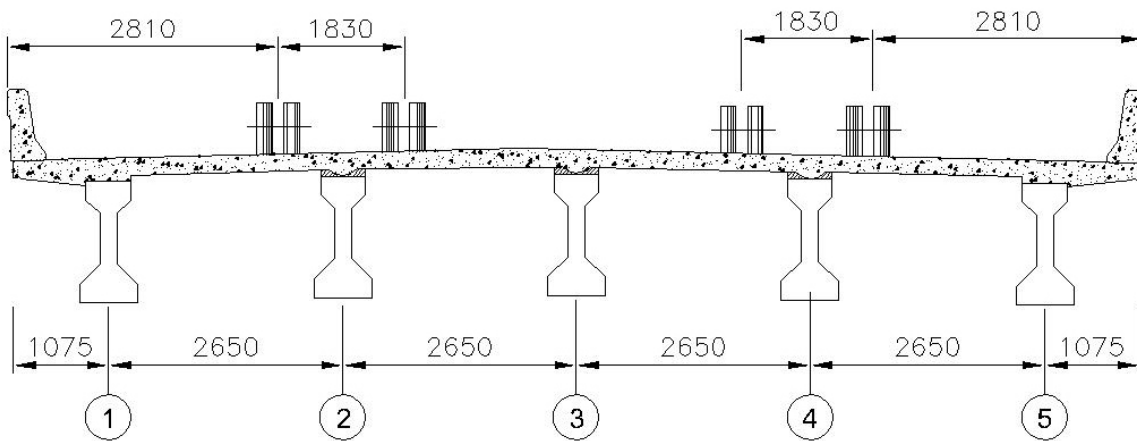


Figure 13 Transversal Position of the Trucks at Test 1

Test 2 and 3, as shown in Figure 14, Figure 15b and Figure 15c, were indented to produce maximum deflection of Girder 2 and to examine the deflection of the deck at targets 17 and 18 (see Figure 7). Additional details of the load tests configurations are summarized in Figure 15.
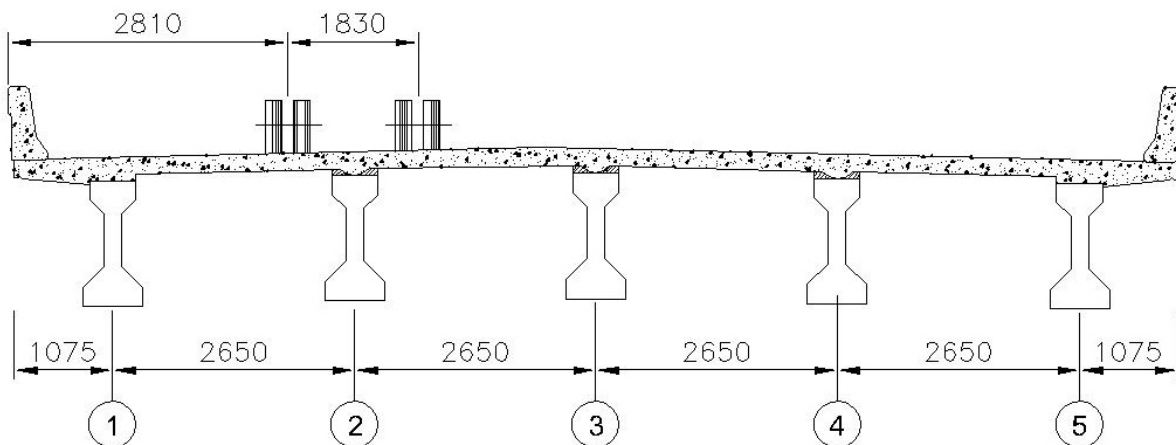


Figure 14 Transversal Position of the Trucks at Tests 2 to 3

A "zero reading" (i.e. bridge without trucks) was taken before testing to have the benchmark and at the end of the test to determine any residual deformation. Marks were made on the asphalt to indicate the trucks test configurations following the skew of the bridge. The train of trucks for Test 2 is presented in the picture of Figure 16.

15
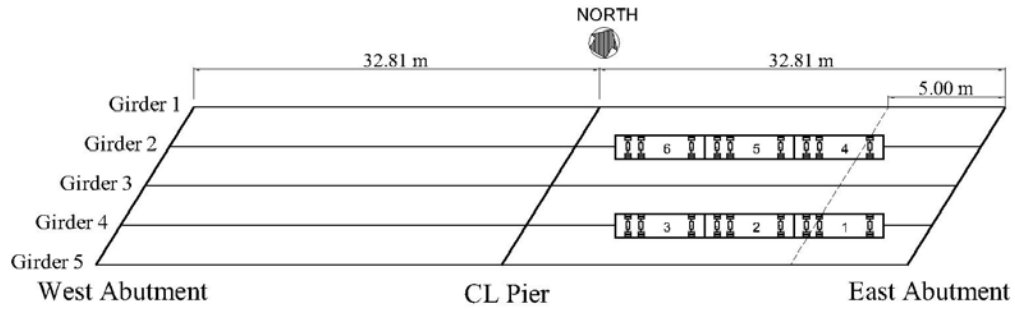
a) Test 1
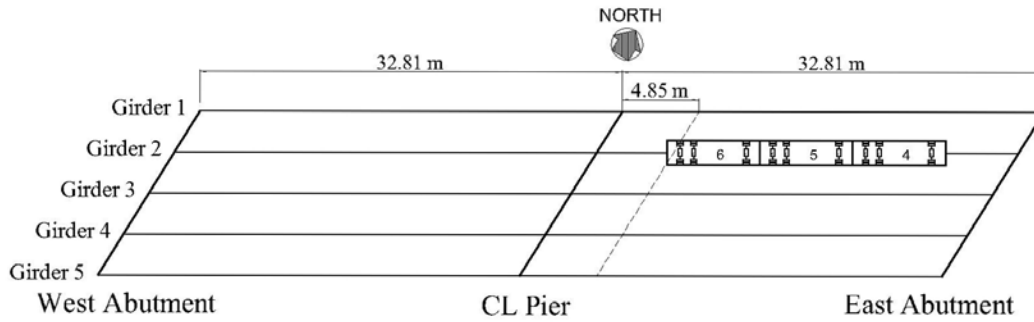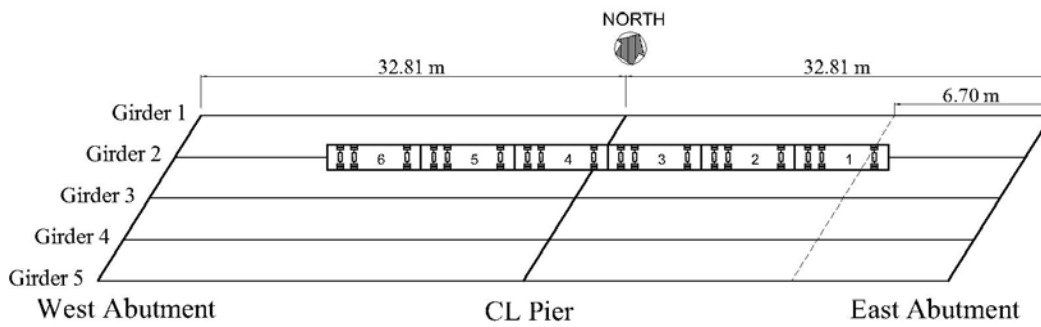

b) Test 2


c) Test 3

Figure 15 Truck Configurations During Load Testing of Bridge B-20-133 (Drawing not to scale)



Figure 16 Trucks Aligned During Test 2

16

Once the total station was leveled and acclimatized, initial readings were taken for each target. Afterwards, the trucks drove to the configuration of test 1. At each stop, before acquiring data, ten minutes lapsed to allow for potential settlements. To assure stable measurements, two readings were taken for each target in order to average out errors. Once the readings were taken, the trucks moved to the next stop and the same procedure was repeated. No strain data were collected during the static tests due to equipment problems.

### 2.2.2 Bridge B-20-134

For this bridge, four load configurations identified as Test 1, 2, 3 and 4 were planned to produce maximum deflections. Test 1 was intended to produce maximum deflection of Span 2. Two trains of three trucks were transversally placed and centered on Girders 2 and 4 of the bridge, as it is shown in the sketches of Figure 17 and Figure 19a.
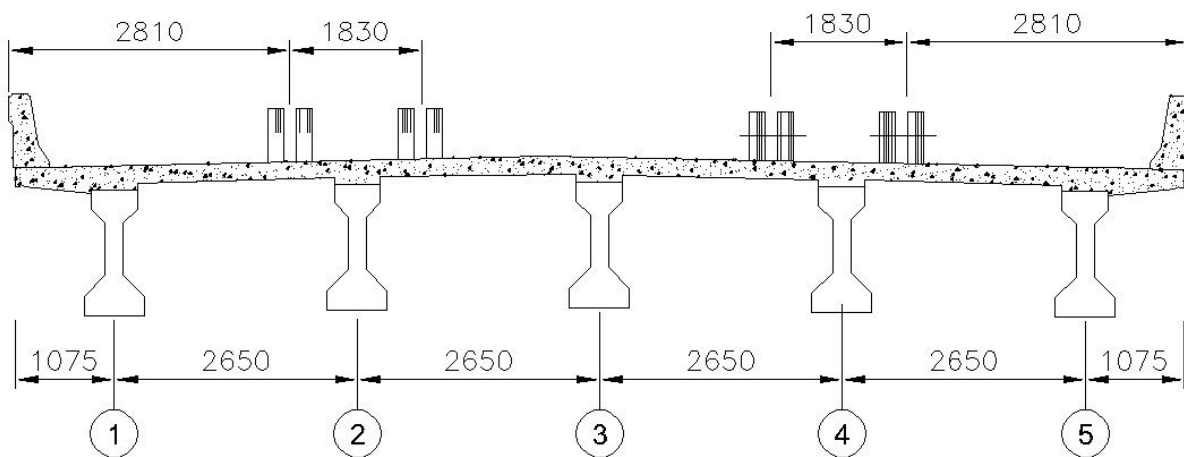


Figure 17 Transversal Position of the Trucks for Test 1

Tests 2, 3 and 4, see Figure 18, were indented to produce maximum deflection of girders at span 2. Details of the stops are summarized in Figure 19b through Figure 19d respectively.
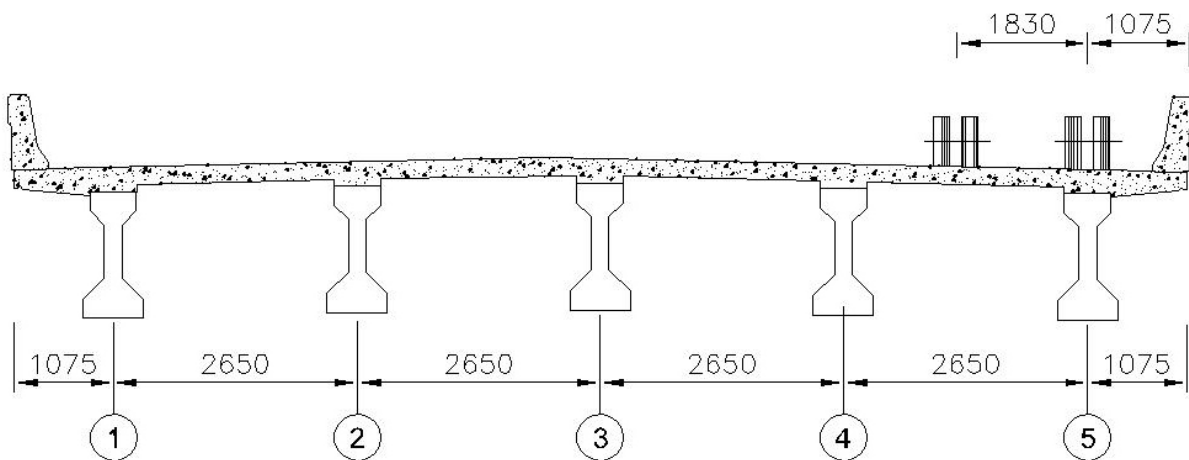


Figure 18 Transversal Position of the Trucks for Tests 2 to 4

17

a) Test 1

b) Test 2

c) Test 3
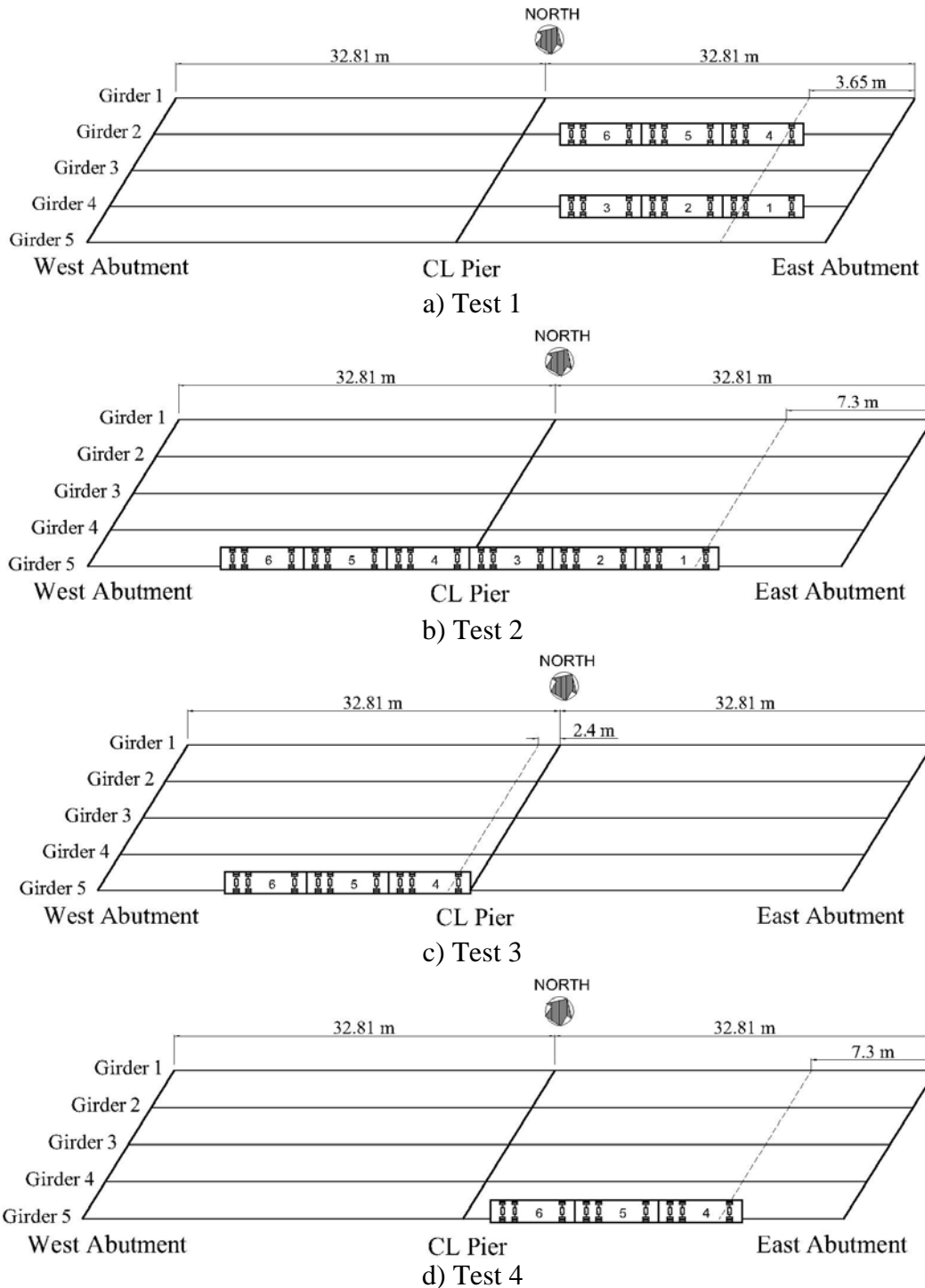
d) Test 4

Figure 19 Truck Configurations During Load Testing of Bridge B-20-134 (Drawing not to scale)

Before the test started, a "zero reading" (i.e. the bridge was not loaded) was taken to be the benchmark and at the end of the test in order to determine any residual deformation. Marks were made on the asphalt to indicate the trucks configuration of each test. The train of trucks for Stop 1 is shown in the picture of Figure 20.

Figure 20 Trucks Aligned on Test 1

The procedure followed for bridge B-20-133 was repeated. Strain data were collected during the first three load configurations (Tests 1 to 3).

## 2.3  Test Results

### 2.3.1  Bridge B-20-133

The vertical deflections resulting from the load tests are given below. Figure 21 shows the deflection of Girder 1 corresponding to the load configurations of Figure 15.  The origin of the "z" axis in the plot of Figure 21 is located at the left support (west abutment) of the girder. The first point plotted in Figure 21 represents the experimental values obtained at target 11 during each test (see Figure 7). Target 11 was located at a distance equal to 1.10 m from the west abutment toward the central pier.
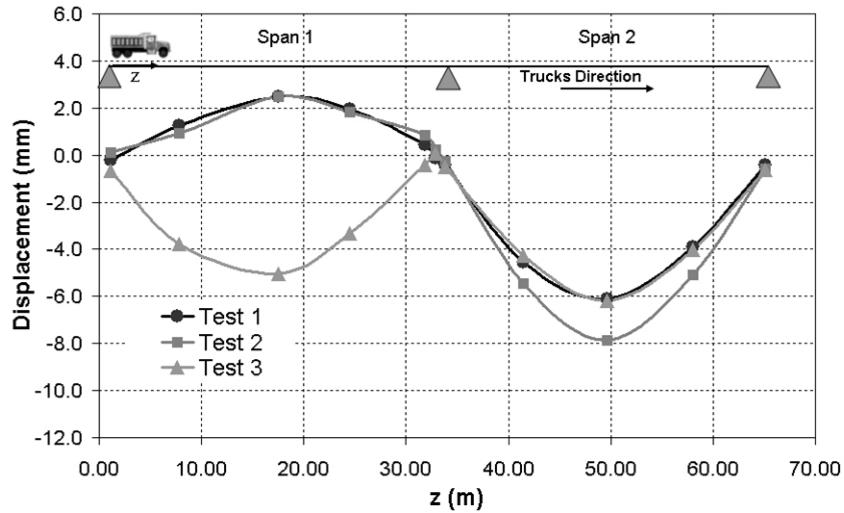


Figure 21 Longitudinal Deflections Girder 1 Tests 1 to 3

A preliminary examination of the data indicates that the readings are accurate.  The consistency of the readings from test to test gives credence to their validity.  The curves also exhibit, in general, a good transition from point to point. The value of the vertical displacement of Girder 1 for test 1 was lesser than its corresponding value during test 2. This difference is explainable considering that during test 2 there was only one train of trucks loading span 2 and it was located directly over Girder 2 (close to Girder 1).  The vertical displacement of Girder 1 during test 3 is asymmetric because the load condition was not symmetrical.

Figure 22 displays the transversal distribution of the girder deflections at a distance L/2 from the central pier in Span 2 for each test (Targets 3, 12, 14, 15 and 16). Figure 23 displays the longitudinal displacement along Girder 3 for Test 1, 2, and 3. For this girder, data were collected only for targets 20, 14 and 19 (see Figure 21). The maximum value of displacement was obtained for the load configuration of test 1 and its value is approximately 10 mm (see Figure 23). This value is below the L/800 recommended by section [2.5.2.6.2] (AASHTO, 1998) which in this case is approximately 41 mm.

20
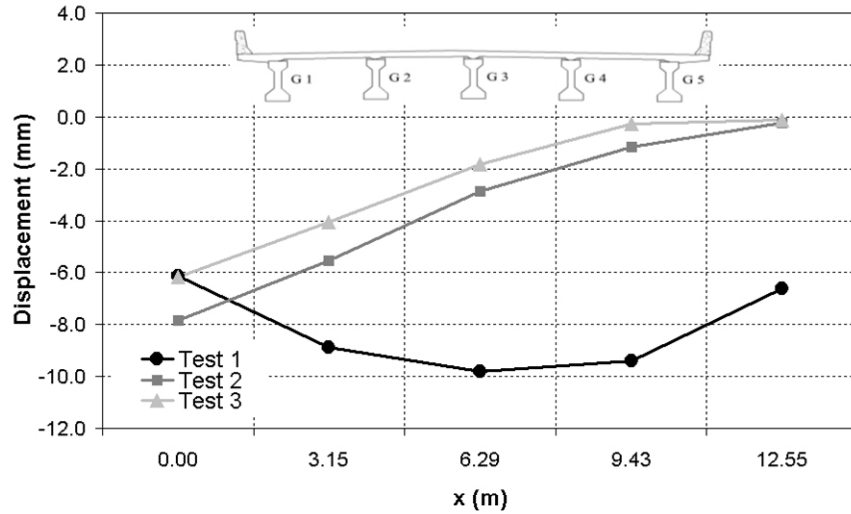
Figure 22 Transversal Deflections at L/2 from West Abutment Tests 1 to 3

Strain measurements were not collected during tests 1, 2 and 3due to equipment problems. Once these problems were solved, a quasi-static test was conducted in order to obtain the range of stresses the FRP components will be subjected during service loads. The test consisted on two trucks driving across the bridge over Girder 4 at a very slow speed and separated each other approximately 15.0 m (50 ft). The quasi-static test was performed acquiring the data only for the strain gages at a frequency of 5 Hz.
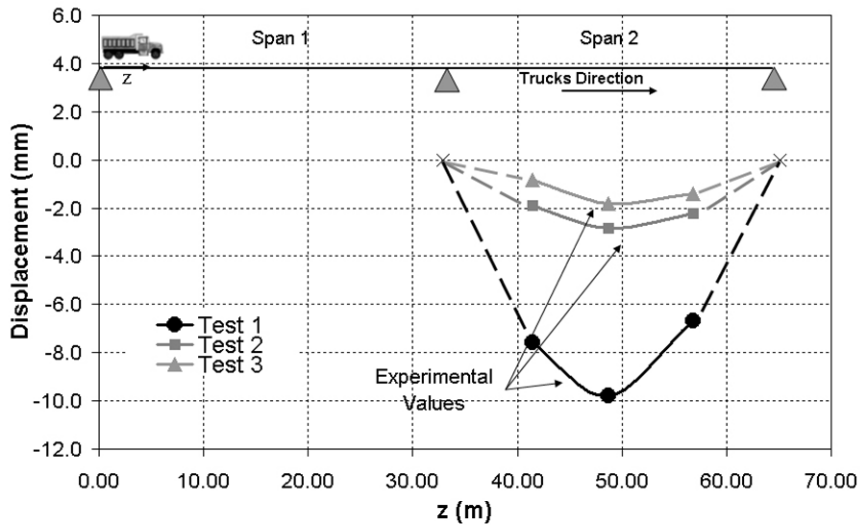


Figure 23 Longitudinal Deflections Girder 3 Tests 1 to 3

Table 5 presents the maximum and minimum strains obtained from the experimental data. The stresses were computed by using the values of the modulus of elasticity obtained from quality control tests that UW elaborated for the FRP components used to reinforce the deck of this Bridge (Bank et al 2005).  Figure 24 shows the strain gage readings retrieved during the quasi-static test. The values correspond to the time when the trucks were driving across the bridge.

21

Table 5 Comparison between Stress Results of FRP Components and Allowable Stress

| Gage | Strain Readings (με) | | Max. Value (με) | Modulus of Elasticity (ksi) * | Computed Stress (ksi) | Allowable Stress (ksi) |
|------|---------|---------|-----------------|-------------------------------|-----------------------|------------------------|
|      | Maximum | Minimum |                 |                               |                       |                        |
| A | 6.0 | -18.0 | 18.0 | 7,100 | 0.128 | 75 |
| B | 7.3 | -15.2 | 15.2 | 7,100 | 0.108 | 75 |
| C | 10.0 | -13.0 | 13.0 | 5,700 | 0.074 | 80 |
| E | 6.0 | -14.0 | 14.0 | 5,100 | 0.071 | 80 |
| F | 9.0 | -12.0 | 12.0 | 5,100 | 0.061 | 80 |
| G | 7.0 | -5.0 | 7.0 | 5,680 | 0.040 | 68 |
| I | 6.0 | -17.0 | 17.0 | 5,680 | 0.097 | 68 |

* Bank et al 2005



a) FRP Grid Cross Rods (12.7 mm Diameter )

b) FRP Grid T-bars (50.8 mm)

c) FRP Grid T-bars (50.8 mm)

d) FRP Rebars (25.4 mm Diameter)
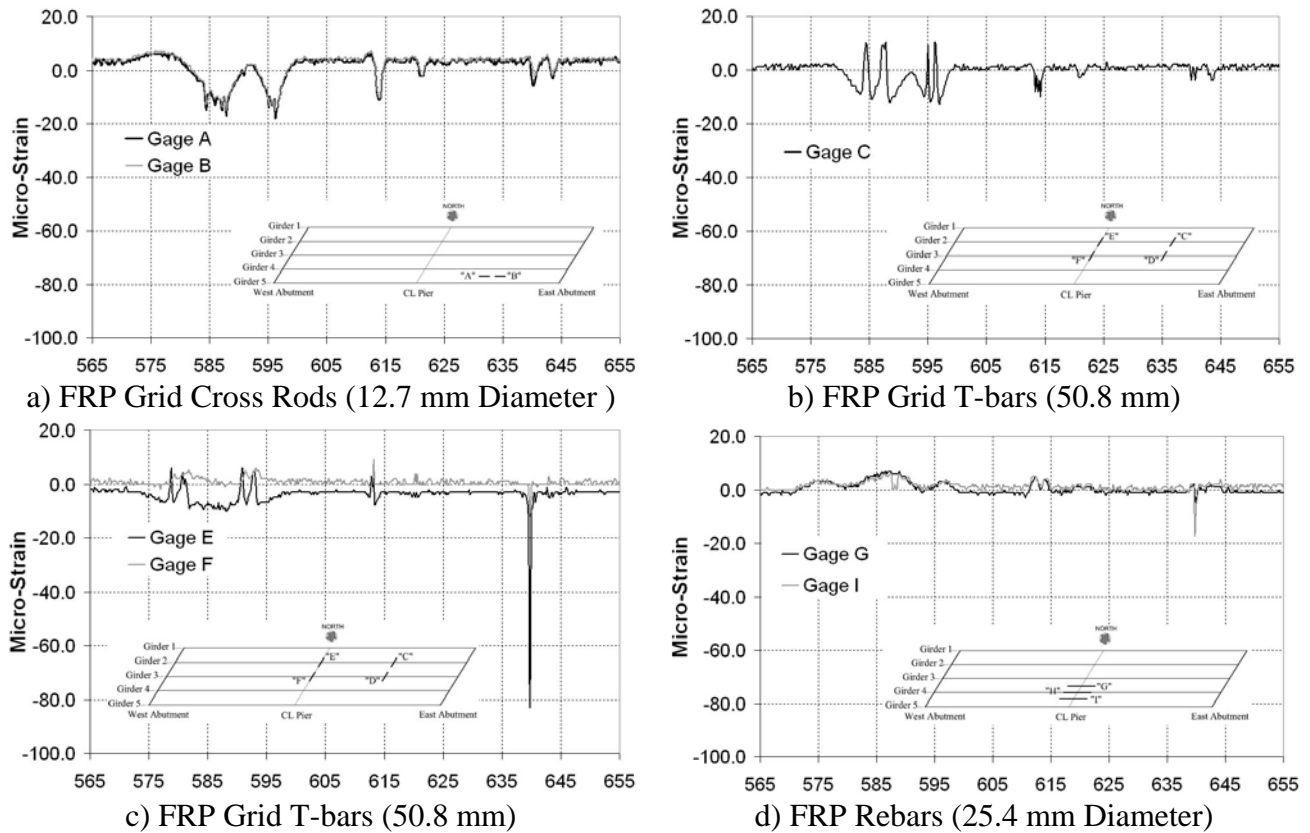
Figure 24 Strain Gage Reading During Quasi-Static Test

In Table 5, the stress values are below the allowable stress limit (as indicated in the material specifications). However, the strain results as plotted appear to be meaningless because of their location relative to the trucks. In fact, the trucks drove over Girder 4 and the strain gage readings were taken (see Figure 9) on the opposite side of the deck. The trucks moving across the bridge did not produce maximum strains readings at the gage locations. In order to obtain the maximum values of the experimental strains and to compare them to the analytical ones, the trucks should have moved over the girders where the strains were located (over Girders 2 and 3).

## 2.3.2 Bridge B-20-134

The vertical deflections resulting from the load testing are given below.  Figure 25 shows the vertical deflection of Girder 5 corresponding to each test. The curves exhibit a good transition from point to point. The origin of the "z" axis in the plot of Figure 25 is located on the west abutment (left support). In Figure 25, the first point plotted (from left to right) shows the experimental values obtained at target 1 (see Figure 11). This target was located at a distance equal to 1.10 m from the west abutment toward the central pier.
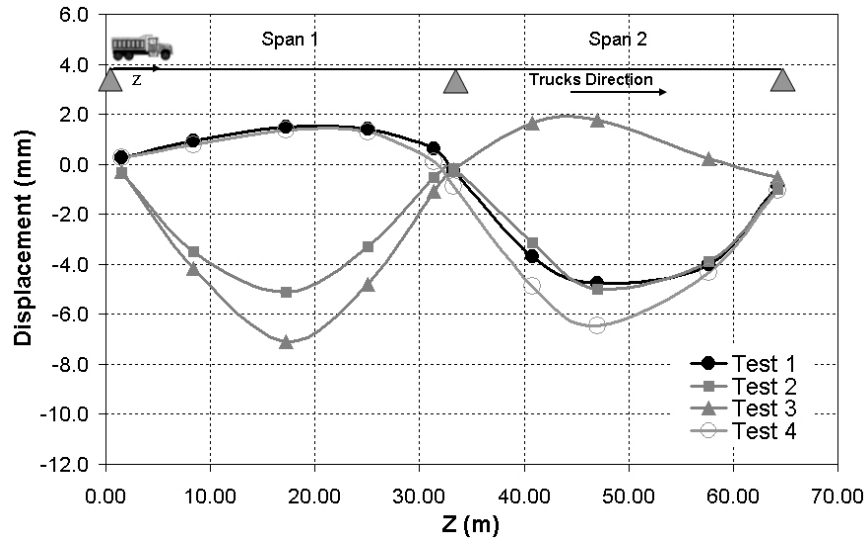


Figure 25 Longitudinal Deflections Girder 5 Tests 1 to 3

The maximum displacement of Girder 5 was obtained for Test 3 and corresponds to approximately 7.0 mm.  Figure 26 displays the transversal distribution of the girders deflection at mid-span 2 (Targets 8, 11, 12, 13 and 14 on Figure 11). The origin of the x-axis is target 8 (first point plotted from left to right) and the distance between each target corresponds to the girder spacing computed according to the north and east coordinates saved by the RTS.
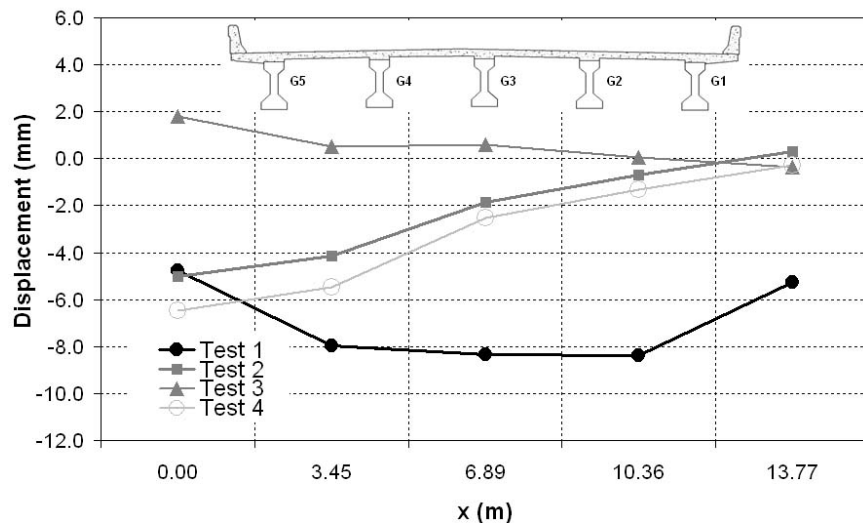


Figure 26 Transversal Deflections at L/2 from west abutment Stops 1 to 3

23

Figure 27 shows the longitudinal displacement along Girder 3 for the load configurations of tests 1, 2, 3 and 4. For this girder, data were only collected for targets 18, 12 and 19 (see Figure 11). The maximum value of displacement was obtained for the load configuration of test 1 and its value is approximately 8 mm. This value is below the L/800 recommended by section [2.5.2.6.2] (AASHTO, 1998) which in this case is approximately 41 mm.
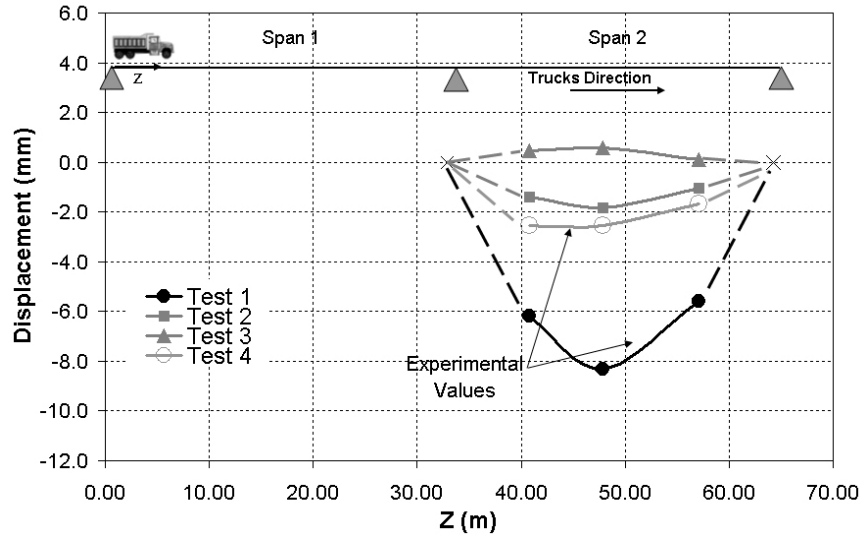


Figure 27 Longitudinal Deflections Girder 3 Tests 1 to 4

Figure 28 shows the strain gage data acquired during test 2 and test 3. Test strains are compared to the one obtained by a FEM simulation of Tests 2 and 3. Table 6 summarizes the average values of all the readings collected for each configuration. For both tests and FEM simulations, the maximum strains in the reinforcement are way below the yield limit. In this bridge, the location of the gages relative to the trucks is appropriate, but the readings are not representative of cracked sections.
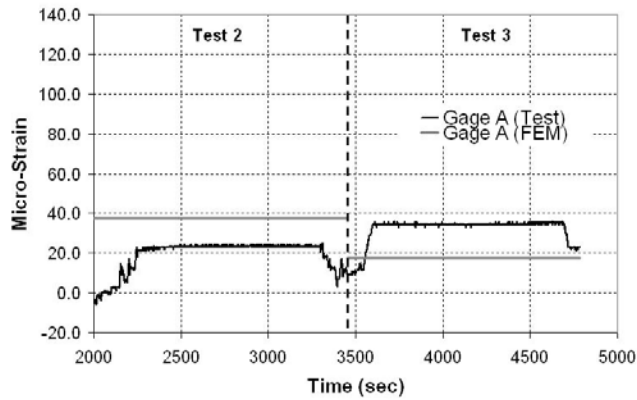
a) Longitudinal reinforcement
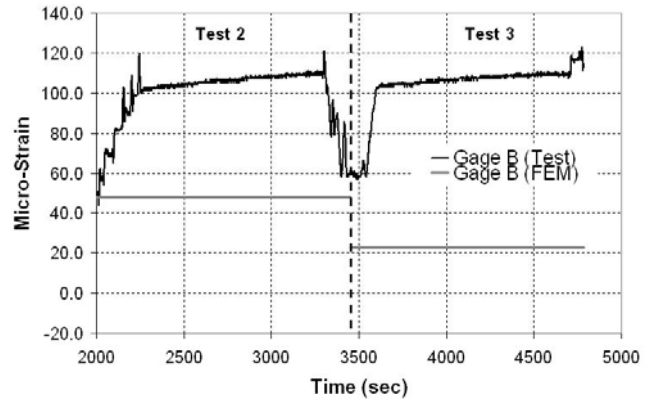


b) Longitudinal reinforcement
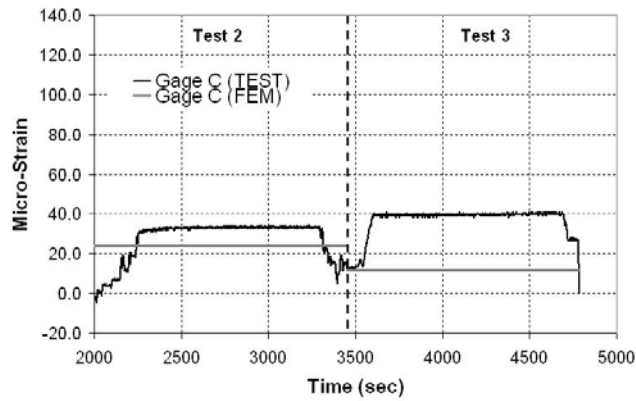


c) Longitudinal reinforcement

Figure 28 Strain Gage Reading during Static Test

Table 6 Maximum Strains (Tests 1 to 3).

| Gage | A (με) | B (με) | C (με) |
|---|---|---|---|
| Test 2 (Experimental) | 25.0 | 121.0 | 34.0 |
| Test 2 (FEM) | | | |
| Test 3 (Experimental) | 36.0 | 123.0 | 41.0 |
| Test 3 (FEM) | | | |

## 2.4 Discussion of Results

### 2.4.1 Bridge B-20-133

The experimental deflections of Girder 1 were compared to the results based on a 1-D beam analysis. The girder distribution factor, GDF (defined as the ratio of the maximum moment on a girder at a given live load condition, and the maximum theoretical moment determined by applying the entire load truck to a single composite section), were determined according to the AASHTO LRFD Bridge Design Specifications (1998) [section 4.6.2.6]. A multiple presence factor m=1 was assumed when using the lever rule. Details of calculation are summarized in Table 7 and Table 8.

Table 7 GDFs as per AASHTO LRFD Bridge Design Specifications (1998)

| Girder No. | No. of Lanes Loaded | AASHTO Formula | GDF Spans 1 and 2 |
|---|---|---|---|
| 1, 5 | 2 | $GDF_E = e.GDF_{2,4}, \ e = 0.77 + \dfrac{d_e}{2800} = 0.997$ | 0.66[a] |
| 2, 3, 4 | 2 | $GDF_I = \left(0.075 + \left(\dfrac{S}{2,900}\right)^{0.6} \left(\dfrac{S}{L}\right)^{0.2} \left(\dfrac{K_g}{L*ts^3}\right)^{0.1}\right).R_f$ | 0.67[a] |
| 1, 5 | 1 | $GDF_E.P = \left[\left(\dfrac{P}{2}\right)e_1 + \left(\dfrac{P}{2}\right)e_2\right]*\dfrac{1}{S}$ ; (Lever rule) | 0.66 |
| 2, 3, 4 | 1 | $GDF_I = \left(0.06 + \left(\dfrac{S}{4300}\right)^{0.4} \left(\dfrac{S}{L}\right)^{0.3} \left(\dfrac{K_g}{L*t_s^3}\right)^{0.1}\right).R_f$ | 0.46[a] |

[a] See NOTATIONS for parameters and units

Table 8 Input Data for Calculations of GDFs (AASHTO, 1998)

| Parameter | Definition | Value |
|---|---|---|
| $S$ (mm) | Girder spacing | 2650 |
| $L$ (mm) | Span length | 32810 |
| $I$ (mm$^4$) | Moment of inertia of the concrete girder section | $1.0806*10^{11}$ |
| $E_s$ (MPa) | Modulus of elasticity of concrete girder | 30669 |
| $E_{cs}$ (MPa) | Modulus of elasticity of concrete slab | 24855 |
| $A$ (mm$^2$) | Cross sectional area of girder | 507300 |
| $e_g$ (mm) | Distance between center of gravity of girder and deck | 842.50 |
| $t_s$ (mm) | Thickness of concrete deck | 200 |
| $\theta$ deg | Skew angle | 32.17 |
| $d_e$ (mm) | Distance between center of exterior girder and barrier edge | 635 |
| $K_g$ (mm$^4$) | $K_g = n(I + Ae_g^2)$ | $5.7764*10^{11}$ |
| $n$ | $n = E_s / E_{cs}$ | 1.234 |
| $C_1$ | $C_1 = 0.25\left(\dfrac{K_g}{Lt_s^3}\right)^{0.25}\left(\dfrac{S}{L}\right)^{0.5}$ | 0.0865 |
| $R_f$ | $R_f = 1 - C_1(\tan\theta)^{1.5}$ | 0.957 |

For interior girders, the width of the concrete slab section was selected as the average spacing of adjacent girders [4.6.2.6.1], *i.e. S* = 2650 mm.

Figure 29 shows a comparison between the deflections measured at target 12 (Figure 7) of Girder 2 and the analytical deformed shapes of that girder. The deflection measured through the RTS system is generally smaller than the theoretical values, and clearly bellow the L/800 limit of 41 mm [2.5.2.6.2] of each span, as shown in Figure 29a through Figure 29c, thereby demonstrating that serviceability of the bridge is below the AASHTO computed value.



a) Test 1



b) Test 2



c) Test 3
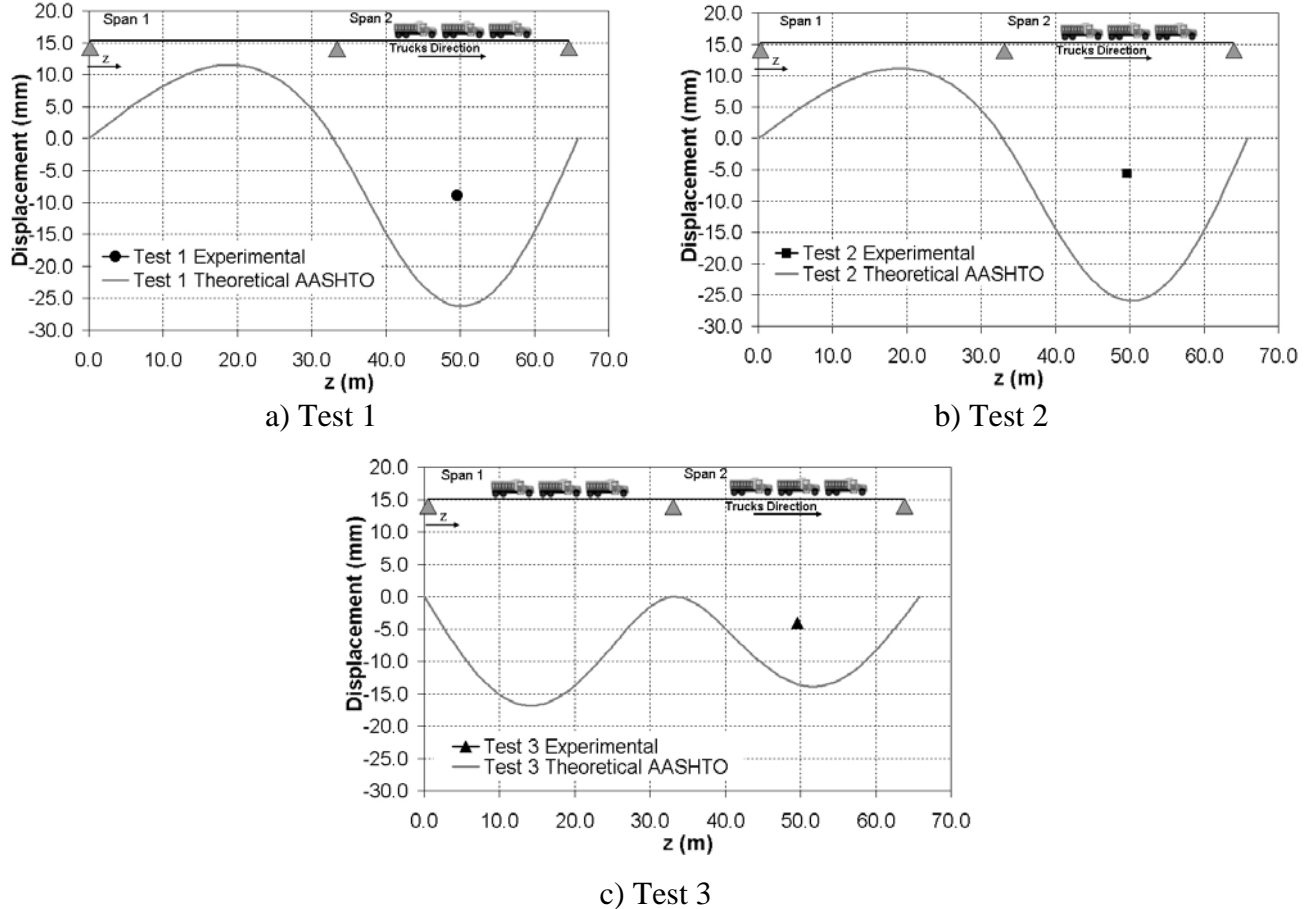
Figure 29 Comparison Between AASTHO Provisions and Experimental Results

The GDF for the *i*th girder at the mid-span of Span 2 was estimated from the deflection data retrieved as:

$$\text{GDF}_i = \frac{\delta_i}{\sum_{j=1}^{5} \delta_j} \tag{1}$$

wherein $\delta_i$=deflection of the ith girder.

Figure 30 and Figure 31 show the GDFs computed for each test taking into account one and two loaded lanes respectively. The curves that correspond to the GDF of the test were computed by

using Eq. (1). Moreover, Figure 30 and Figure 31 allow evaluating the safety factor of the GDF proposed by AASHTO.
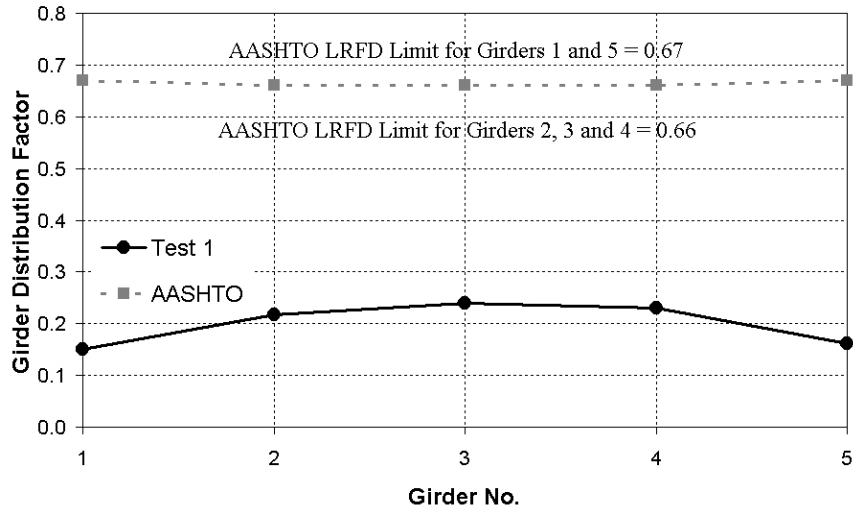


Figure 30 Comparison Between AASHTO and Experimental Girder Load Distribution Factor at Mid-span of Span 2 (Two Lanes Loaded, Stop 1)

The safety factor was computed as the ratio between the analytical GDF proposed by AASHTO and the test GDF obtained by Eq. (1). The minimum safety factor (Girder 3) is equal to 2.75 for the case of two-loaded lanes (Test 1). The minimum safety factor (Girder 1) for the case of one-loaded lane (Test 2 and 3) is equal to 1.33.
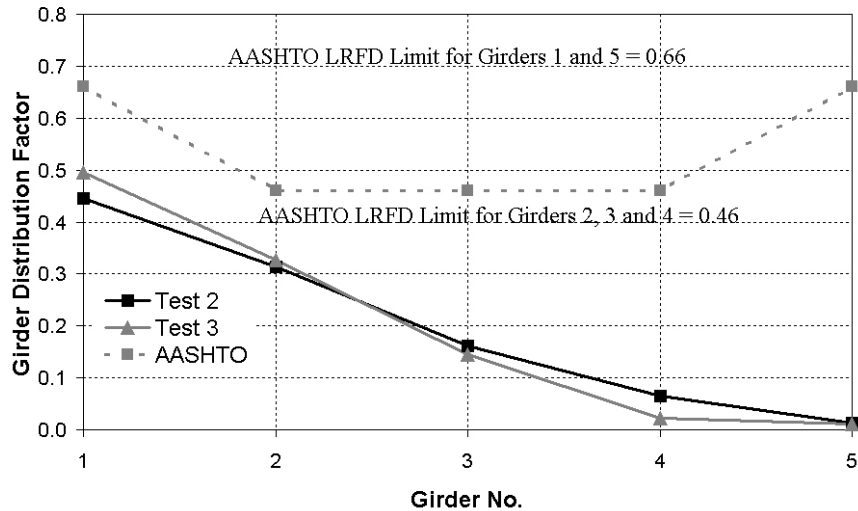


Figure 31 Comparison Between AASHTO and Experimental Girder Load Distribution Factor at Mid-span of Span 2 (One Lane Loaded, Stops 2 and 3)

The GDFs determined experimentally at mid-span 2 (between central pier and east abutment) are always below those based on the AASHTO provisions, which are proven to be conservative for the case under consideration.  One reason  for this difference is in neglecting the transverse stiffening action of the parapets when using the design formulas wherein the thickness of the deck is the only parameter that explicitly accounts for a degree of transverse stiffness in the structural system.

## 2.4.2   Bridge B-20-134

For this bridge, the experimental deflections of Girder 5 were compared to the results based on a 1-D beam analysis. The GDFs were determined according to the AASHTO LRFD Bridge Design Specifications (1998) [section 4.6.2.6]. A multiple presence factor m=1 was assumed when using the lever rule. Details of calculation are summarized in Table 7 and Table 8.

Figure 32a shows a comparison between the deflection measured at target 11 (Figure 11) of Girder 4 and the analytical deformed shapes of that girder. Figure 32b through Figure 32d shows a comparison between the deflections measured on Girder 5 and the analytical deformed shape of the same girder. The deflections measured through the RTS system are generally smaller than the theoretical values, and clearly bellow the L/800 limit of 41 mm [2.5.2.6.2] of each span, as shown in Figure 32a through Figure 32d, thereby demonstrating that serviceability of the bridge is below the AASHTO computed value.
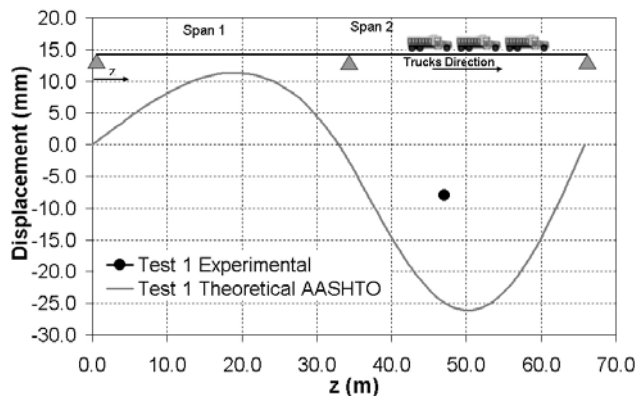


a) Test 1
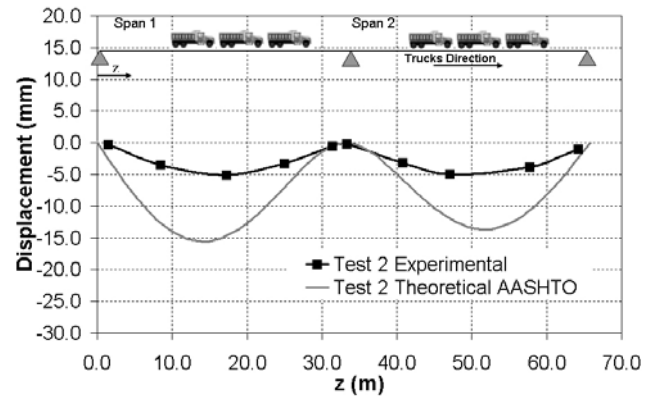
b) Test 2
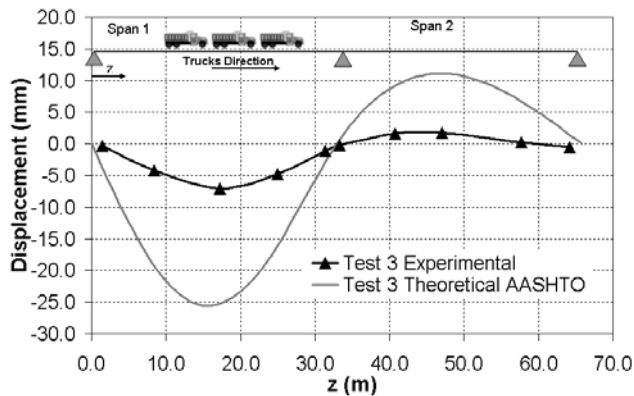
c) Test 3
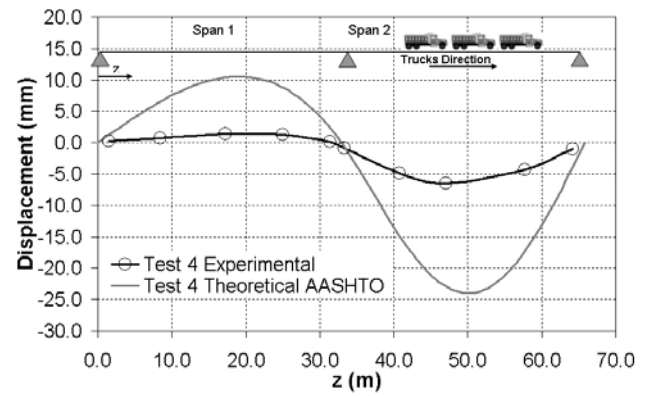
d) Test 4

Figure 32 Comparison Between AASTHO Provisions and Experimental Results

The GDF for the *i*th girder at the mid-span 2 was estimated from the deflection data recorded during the load test by using Equation (1). Figure 33 and Figure 34 show the girder distribution factors obtained for each test taking into account one and two loaded lanes respectively.
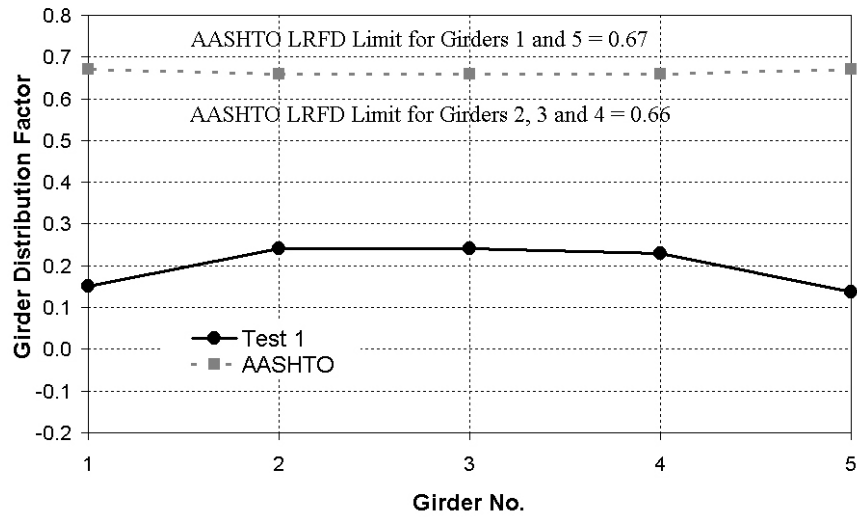
Figure 33 Comparison Between AASHTO and Experimental Girder Load Distribution Factor at
Mid-span of Span 2 (Two Lanes Loaded, Stop 1)
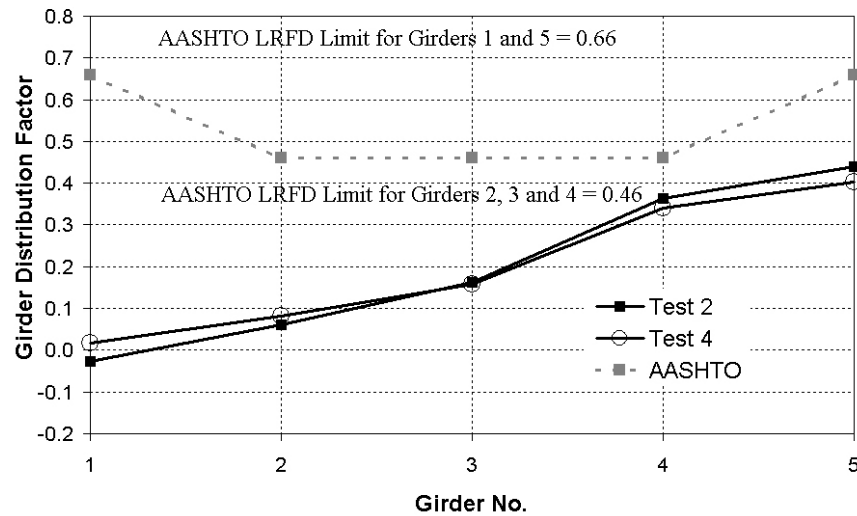


Figure 34 Comparison Between AASHTO and Experimental Girder Load Distribution Factor at
Mid-span of Span 2 (One Lane Loaded, Stops 2 and 3)

For both bridges, the load distribution factors determined experimentally at mid-span 2 (between
central pier and east abutment) are always below those computed based on the AASHTO
provisions, which for the case of bridge B-20-134 are also proven to be conservative.

## 2.5 Finite Element Method Simulations

FEM simulations were created based upon the data obtained from the diagnostic test. These numerical models may be used to approximate the bridge's behavior to limiting loads. A three-dimensional model of the main structural elements was used. The model consisted of 3-D solid elements that represented the deck and girders and parapets acting as a composite structure. The spacing used between the girders was the same as the one on the actual bridge. For a truck placed anywhere on the deck, the mesh allowed accurate transverse distribution of wheel loads to the girders. A depiction of the finite-element mesh used for both bridges is shown in Figure 35.
The FEM Models were implemented by using the commercial software Abaqus 6.4. A linear elastic analysis was performed for each of the load configurations of each bridge.
The finite element used for the simulations was the so-called "C3D8" which is a continuum (solid) 3-D element that has eight nodes with three active degrees of freedom (DOF) per node. The active degrees of freedom are the translations along each of the global coordinate axis (x, y and z-axis).
The contribution of the parapets (or barrier rails) resisting live loads has been considered by other researches (Cai, 2004) and their effect was taken into account in the FEM Models. In order to consider the difference of the stiffness of the concrete elements that constitute the bridge structure (girders, deck and parapets), three different materials were defined in the FEM Model. The concrete of the deck was taken into account as having an f'c equal to 38 MPa (5500 psi), the concrete of the parapets was modeled with a f'c equal to 28 MPa (4000 psi) while the concrete of the girders was modeled with a f'c equal to 42 MPa (6090 psi). The effect of the diaphragms was not implemented in the FEM Model. Figure 35 shows a detail of the mesh at the right support (east abutment). The supports (central pier, west and east abutments) were modeled as fixed supports (three DOF restricted). The loads of the trucks were applied as concentrated loads at nodes that coincided with the location of the truck wheels during the tests.
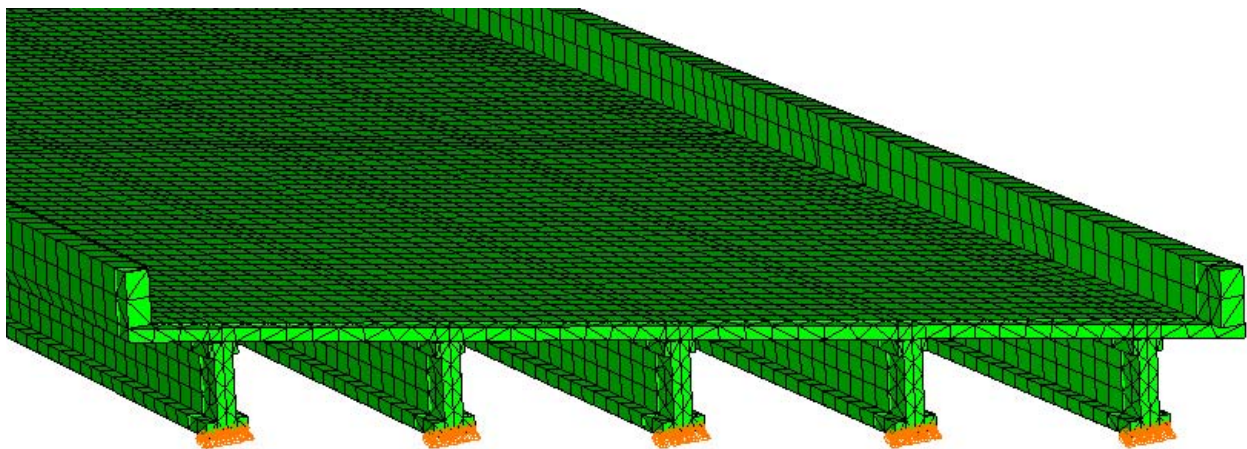


Figure 35 Finite Element Model of the Bridge

### 2.5.1 Bridge B-20-133

Figure 36 compares the FEM Model results to those directly measured in the field for Tests 1 to 3 for the external Girder 1 of bridge B-20-133. The numerical model was found to be adequately accurate describing the longitudinal deflections measured in the field.



a) Test 1



b) Test 2



c) Test 3
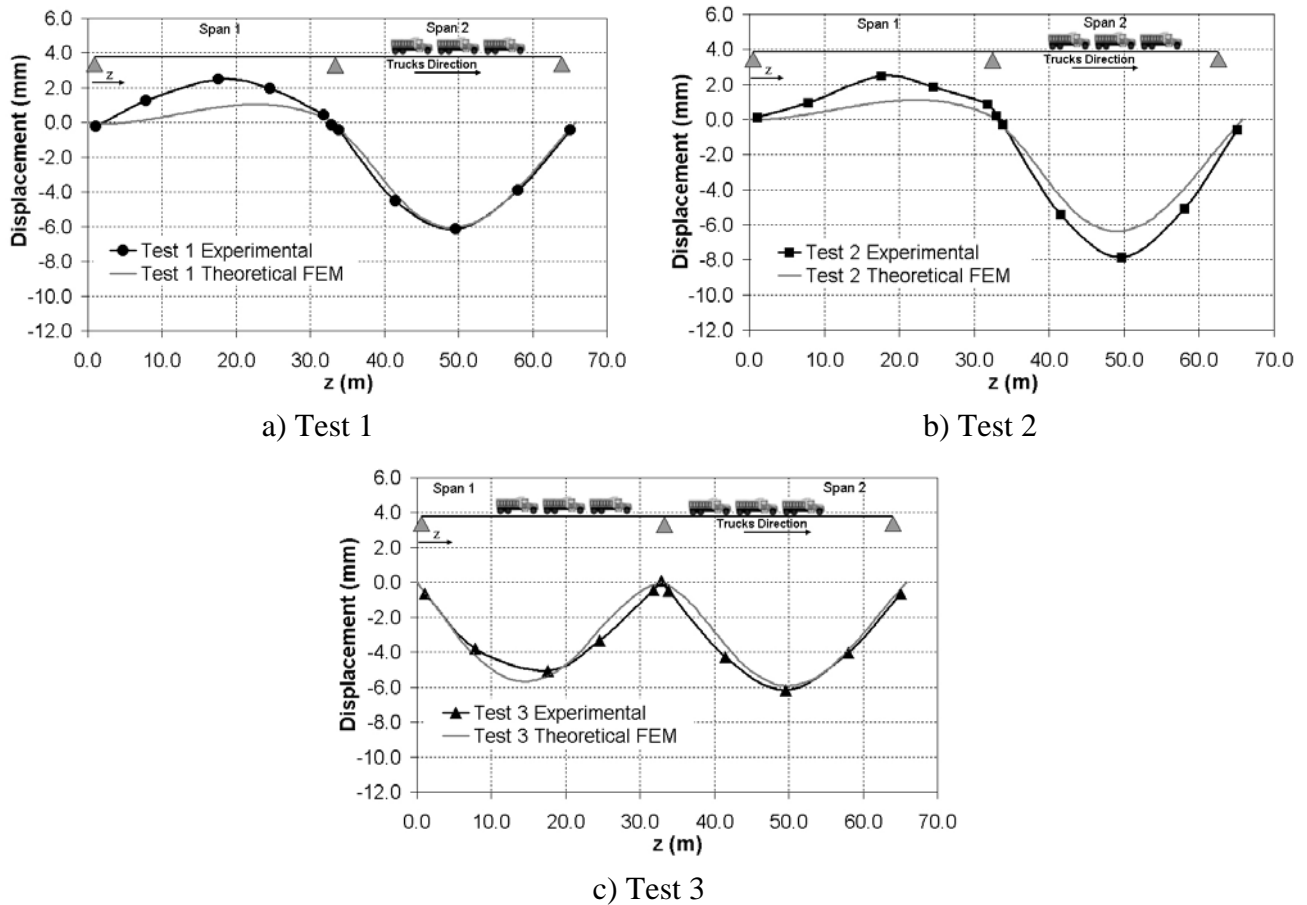
Figure 36 Comparison between FEM Model and Experimental Results (Test 1 to 3)

The transversal deflections are compared in Figure 37. For this bridge, the model showed its effectiveness predicting transversal experimental distribution of deflections.
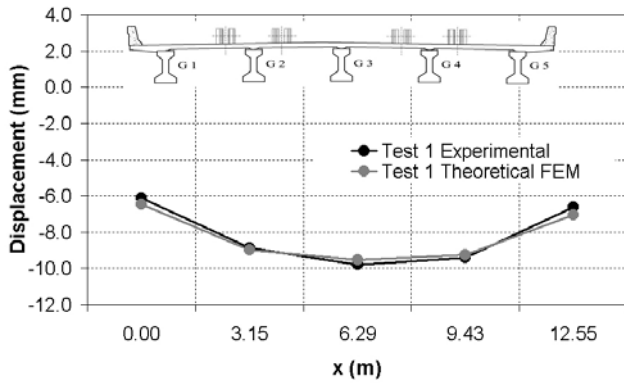


a) Test 1
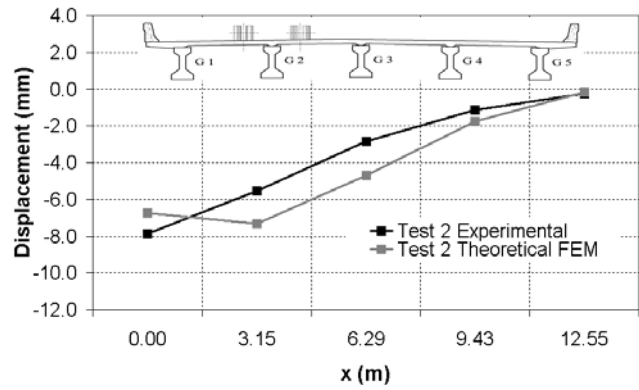
b) Test 2
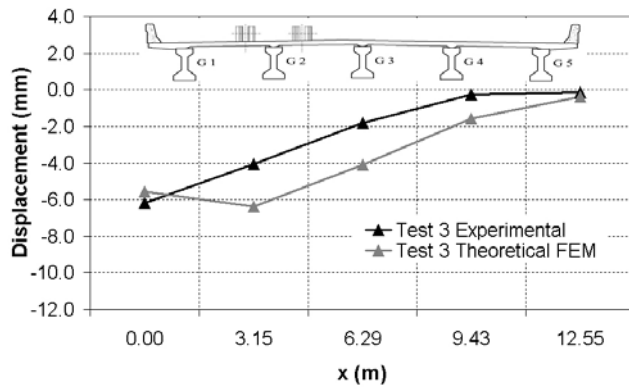
e) Test 3

Figure 37 Comparison between FEM Model and Experimental Results (Transversal Deflections at L/2 from central pier, Tests 1 to 3)

### 2.5.2 Bridge B-20-134

Figure 38 compares the FEM results of the external Girder 5 to those directly measured in the field for the load configurations of the tests 1 to 4. The numerical model was found to be adequately accurate describing the longitudinal deflections measured in the field.
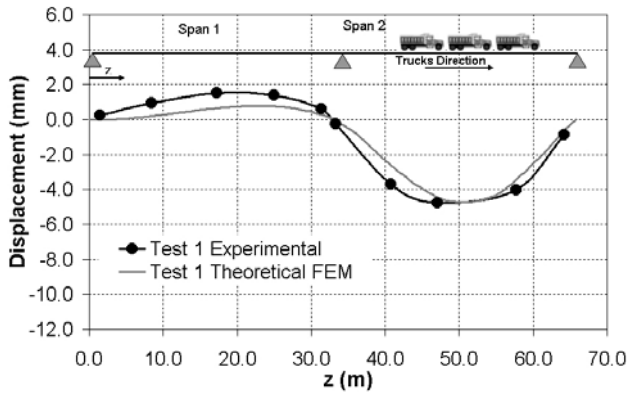


a) Test 1
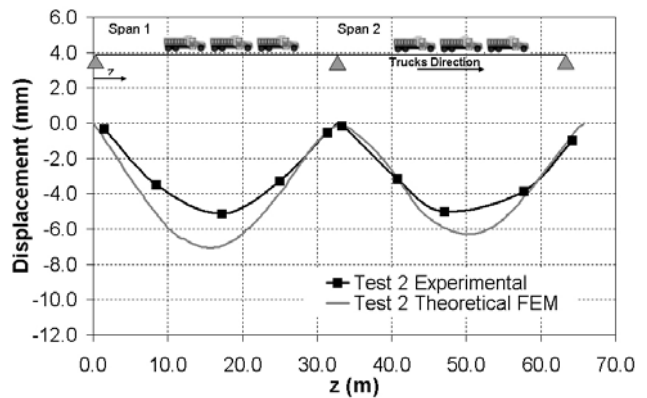
b) Test 2
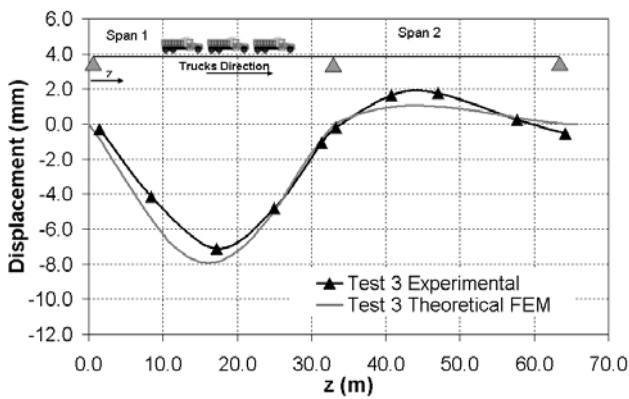
c) Test 3
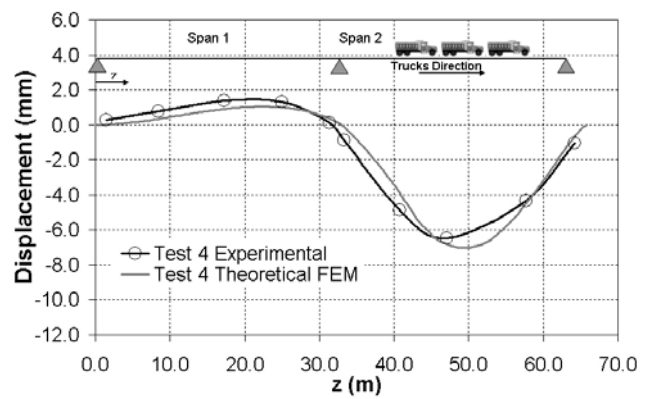
d) Test 4

Figure 38 Comparison between FEM Model and Experimental Results (Tests 1 to 4)

Figure 39 compares the transversal deflections computed by the FEM Model to the experimental ones. The results indicate that the model also showed its effectiveness predicting transversal experimental distribution of deflections for bridge B-20-134.



a) Test 1

b) Test 2

c) Test 3

d) Test 4
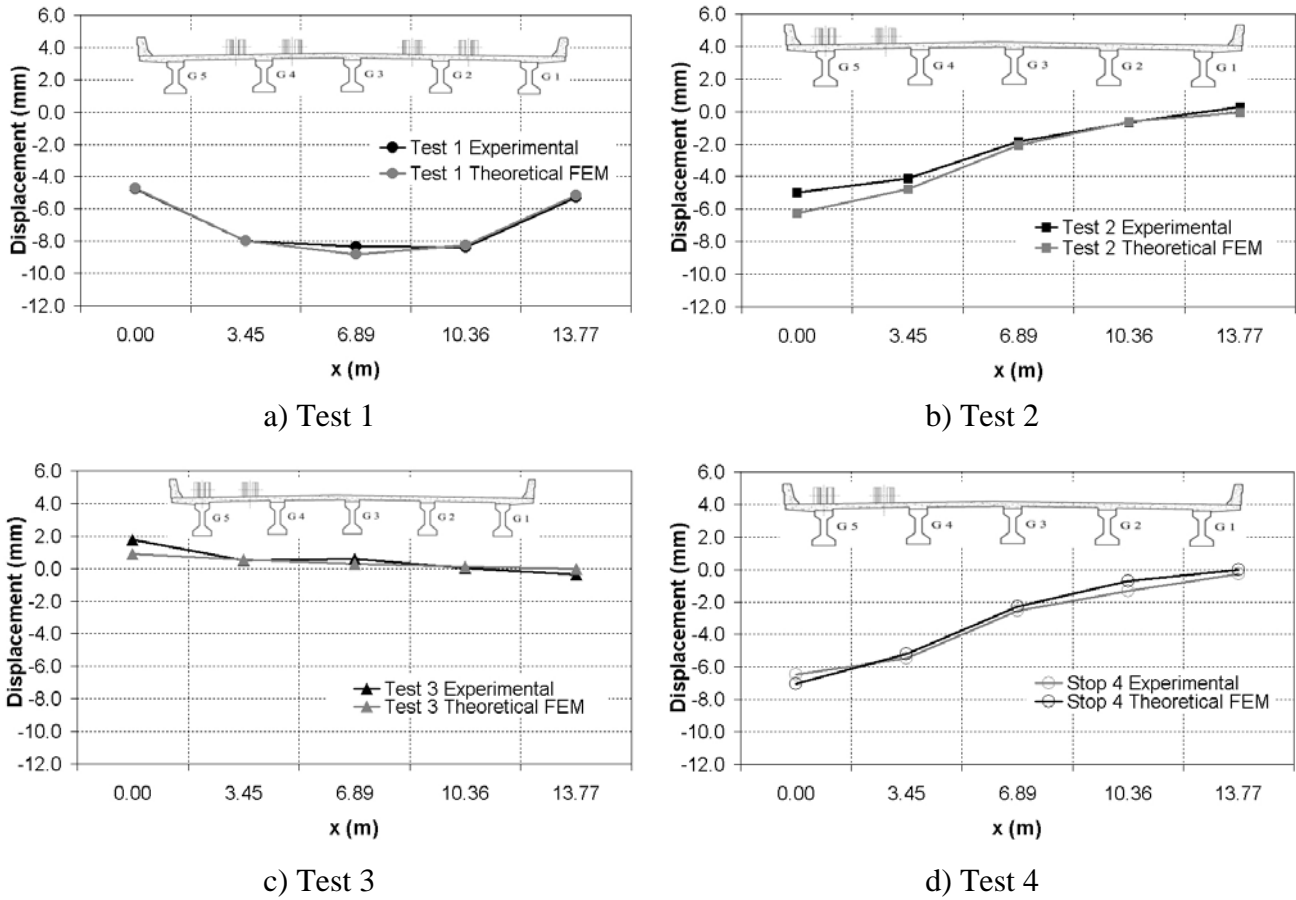
Figure 39 Comparison between FEM Model and Experimental Results (Transversal Deflections at L/2 from central pier, Tests 1 to 4)

# 3 SUMMARY AND CONCLUSIONS

Conclusions based on the deflection and strain measurements via Robotic Tacheometry System (RTS) and Data Acquisition System (DAS) respectively during the diagnostic load test and the comparison to analytical results based on the AASHTO LRFD Bridge Design Specifications (1998) and the numerical results based on the FEM simulations of both bridges can be summarized as follows:

- The structural assessment confirms a good response of the bridges for the serviceability, since the experimental deflections were found to be smaller than the theoretical values determined according to the design provisions (AASHTO, 1998).

- The transversal deflection distribution computed according to the AASHTO provisions diverges from the actual transversal distribution of the bridge yielding to a safe design that does not predict or evaluate the actual load carrying capacity of the structure.

- In order to obtain a benchmark for the long term monitoring of the bridges B-20-133 and B-20-134, a load test was conducted. Girder deflections and strain gage data were recorded for different trucks configurations.

- The use of the RTS confirms its cost-effectiveness for deflection measurement. The fact that the technology allows for non-contact measurement significantly enhances its versatility.

- The deflection data collected with the RTS indicates that the readings were accurate and the consistency of the readings gives credence to their validity.

- The experimental strain data obtained with the DAS are not useful to determine the safety of the structure since the load configuration used during the quasi-static test of the bridge was not the most appropriate to produce the maximum strains the structure would be subjected during its serviceability.

- A Finite Element model was developed. The model was able to represent the actual behavior of the bridge and can be used to determine the actual load rating of the bridges and therefore their safety over time.

- The results of the FEM analysis confirmed that the assumption of composite action between deck and girders is adequate to describe the response of the bridge during the load test.

In the future, if another load test is to be conducted, special attention should be given to monitoring the degradation of any constituent of the bridge to determine the actual load rating of the structure.

# 4    REFERENCES

American Association of State Highway and Transportation Officials (AASHTO), (1996): ''LRFD standard specifications.'' 16th Ed., Washington, D.C.

American Association of State Highway and Transportation Officials (AASHTO), (1998): ''LRFD bridge design specifications.'' 2nd Ed., Washington, D.C.

American Association of State Highway and Transportation Officials (AASHTO), (2002): "Standard Specifications for Highway Bridges", 17th Edition, Published by the American Association of State Highway and Transportation Officials, Washington D.C.

American Concrete Institute (2005), "Guide for the Design and Construction of Concrete Reinforced with FRP Bars," ACI 440.1R-05, American Concrete Institute, Farmington Hills, MI.

Bank, L.C., Oliva, M.G., Russel, J.S., Dieter, D.A., Dietsche, J.S., Berg, A.C., Ehmke, F.G., "Bridge B-20-133 on U.S. 151 with Fiber Reinforced Polymer Reinforced Concrete Deck". Final Report. University of Wisconsin-Madison, January 2005.

Bank, L., Oliva, M., Russell, J., Jacobson, D., Conachen, M., Nelson, B., and McMonigal, D. (2004), "Super-Sized Double-Layer Pultruded Gratings," COMPOSITES 2004 Convention and Trade Show, American Composites Manufacturers Association (ACMA), Oct. 6-8, 2004, Tampa, FL, CD-ROM.

Bank, L.C., and Xi, Z. (1993), "Pultruded FRP Grating Reinforced Concrete Slabs," Fiber-Reinforced-Plastic for Concrete Structures - International Symposium (eds. A. Nanni and C.W. Dolan), SP-138, American Concrete Institute, Farmington Hills, MI, 561-583.

Bank, L.C., and Xi, Z. (1995), "Punching Shear Behavior of Pultruded FRP Grating Reinforced Concrete Slabs,"  Non-metallic (FRP) Reinforcement for Concrete Structures (ed. L. Taerwe), RILEM Proceedings 29, E&FN Spon, London, 360-367.

Bank, L.C., Xi, Z., and Munley, E. (1992), "Performance of Doubly-Reinforced Pultruded Grating/Concrete Slabs," Proceedings of the 1st International Conference for Advanced Composite Materials in Bridges and Structures (eds. K.W. Neale and P. Labossiere), October 6 9, Sherbrooke, Canada, Canadian Society for Civil Engi-neering, 351 360.

Barker, M. G., and Schrage, S. D. (2000): ''High performance steel: design and cost comparisons.'' Modern Steel Constr., 16, 35–41.

Barth, K. E., Roeder, C. W., Christopher, R. A., and Wu, H. (2004): ''Evaluation of live load deflection criteria for I-shaped steel bridge design girders.'' Proc., Int. Conf. on High Performance Materials in Bridges, Kona, Hawaii, ASCE, Reston, Va.

Bradberry, T.E. (2001), "Fiber-reinforced-plastic Bar Reinforced Concrete Bridge Decks," Proceedings of the 80th Annual Transportation Research Board Meeting, Jan. 9-13, 2001, Washington, DC, CD #01-3247.

Berg, A. (2004). "Analysis of a bridge deck built on U.S. Highway 151 with FRP Stay-in-Place Forms, Grids, and Rebars", Master Thesis, University of Wisconsin-Madison, 2004.

Conachen, M. (2005). "Modular 3-D FRP Reinforcing System for a Bridge Deck in Fond du Lac, Wisconsin", Master Thesis, University of Wisconsin-Madison, 2005.

Buth, C.E., Williams, W.F., Bligh, R.P., Menges, W.L., and Haug, R.R. (2003), "Performance of the TxDOT T202 (MOD) Bridge Rail Reinforced with Fiber Reinforced Polymer Bars," TTI Research Report 0-4138-3, Texas Transportation Institute, College Station, TX.

Casadei, P. and Nanni, A. (2003); "In-Situ Load Testing of Reinforced Concrete Structures: Case Studies", *South East Asia Construction*, Sept/Oct 2003.

Chajes, M. J., Mertz, D. R., and Commander, B., (1997): "Experimental Load Rating of a Posted Bridge", *Journal of Bridge Engineering*, Vol. 2, No. 1, February 1997, pp. 1-10

Clingenpeel, B. F., and Barth, K. E. (2003). ''Design optimization study of a three-span continuous bridge using HPS70W,'' AISC Eng. J., 39(3), 121–126.

El-Salakawy, E., Benmokrane, B., Masmoudi, R., Brière, F. and Breaumier, E. (2003), "Concrete Bridge Barriers Reinforced with Glass Fiber-Reinforced Polymer Composite Bars," ACI Structural Journal, 100(6), 815-824.

Hill, C. D. and Sippel, K. D. (2002). "Modern Deformation Monitoring: A Multi Sensor Approach." FIG XXII International Congress, Washington DC, USA

Horton, R., Power, E., Van Ooyen, K., and Azizinamini, A. (2000). ''High performance steel cost comparison study.'' Proc., Steel Bridge Design and Construction for the New Millennium with Emphasis on High Performance Steel, Baltimore, 120–137.

Kuhlmann, H. and Glaser, A. (2002). "Investigation of New Measurement Techniques for Bridge Monitoring." 2nd Symposium on Geodesy for Geotechnical and Structural Engineering, Berlin, Germany

Leica Geosystems, Automated High Performance Total Station TCA2003, http://www.leica-geosystems.com

Lynch, R. J. (2004). "Provisional Design Guide in AASHTO Language for FRP Bridge Strengthening", Master Thesis, University of Missouri - Rolla, August 2004.

McDermott, J. F. (1969): ''Local plastic buckling of A514 steel members.'' J. Struct. Div. ASCE, 5(9), 1837–1850.

Merkle, W. J. (2004). "Load distribution and response of bridges retrofitted with various FRP systems", Master Thesis, University of Missouri - Rolla, August 2004.

Nanni, A. (2003), "North American Design Guidelines for Concrete Reinforcement and Strengthening Using FRP: Principles, Applications and Unresolved Issues," Construction and Building Materials, 17(6-7), 439-446.

Roeder, C. W., Barth, K. E., and Bergman, A. (2004). ''Effect of live-load deflections on steel bridge performance.'' J. Bridge Eng., 9(3), 259 – 267.

Roeder, C. W., Barth, K. E., Bergman, A., and Christopher, R. A. (2001). ''Improved live-load deflection criteria for steel bridges.'' NCHRP Interim Rep. No. 20-07/133, National Cooperative Highway Research Program, Washington, D.C.